1982

New polymeric resists for electron beam lithography.

Ameeta Narula
University of Massachusetts Amherst

NEW POLYMERIC RESISTS FOR ELECTRON BEAM LITHOGRAPHY

A Thesis Presented

by

AMEETA NARULA

Submitted to the Graduate School of the
University of Massachusetts in partial fulfillment
of the requirements for the degree of

MASTER OF SCIENCE

SEPTEMBER 1982

POLYMER SCIENCE AND ENGINEERING DEPARTMENT

NEW POLYMERIC RESISTS FOR ELECTRON BEAM LITHOGRAPHY

A Thesis Presented

by

AMEETA NARULA

Approved as to style and content by:

Shaw L. Hsu,
Chairperson of Committee

William J. MacKnight, Head
Polymer Science and Engineering

To my Mother

and Vivek

ACKNOWLEDGEMENTS

I wish to thank my advisor, Dr. S.L. Hsu, for his guidance and support throughout the course of this research. I would also like to extend my appreciation to Dr. G.M. Venkatesh and Dr. G.N. Babu for mumerous and prolonged scientific discussions as well as hours of experimental assistance. Thanks to everyone in the Polymer Science and Engineering Department for making my stay here an enjoyable one. I am also grateful to IBM, East Fishkill Facility for support of this project under contract IBM/CA 623164.

TABLE OF CONTENTS

TABLE OF CONTENTS (Cont.)

LIST OF TABLES

LIST OF FIGURES

LIST OF FIGURES (cont.)

LIST OF FIGURES (cont.)

C H A P T E R I

INTRODUCTION

Multiple thin films which are conducting, insulating and semiconducting are important components of integrated circuit technology. Circuits are fabricated from these layers by patterning the films to form isolated circuit elements which are themselves interconnected by patterned films (1).

The shape and size of the individual elements determine size, ultimate complexity and operating parameters of a finished device. Current applications of integrated circuits require extremely high levels of performance i.e, lower power requirement and higher speed. These requirements are satisfied by using device designs of higher density. To achieve this, it is necessary to improve the lithographic technique (1). This may be done by employing electron beam lithography using specially modified scanning electron microscope. In the past few years, this technique has been widely accepted as a means of producing high resolution patterns by primary pattern generation or direct writing (2).

Lithographic process involves coating the substrate to be patterned with a film of a radiation sensitive polymer termed a resist. The substrate onto which the resist materials are coated is generally a polished silicon wafer coated with a silicon dioxide layer. The oxide layer is about 5000 Å, or less, thick. It acts as a protective coating for the silicon surface and as a dielectric insulation between circuit functions besides being commonly used as a gate in MOS (Metal

Oxide Semiconductor) structures. The resist materials should be compatible with the particular exposure technique (electron, ultraviolet and x-ray radiation) and the subsequent processing. Polymeric resists are used to protect the underlying substrate during etching and metal deposition during pattern fabrication. They are classified into two categories, positive and negative, depending on their repsonse to the exposing radiation. Positive resists degrade and become more soluble in the irradiated area relative to the unexposed area. Negative resists crosslink and become more soluble in the unexposed area. They are characterized by G_S and G_X values respectively. These are defined as the number of scission and crosslinking events taking place respectively per 100 eV of energy absorbed.

The resist material must satisfy the following requirements (3,4,5):

1. High Sensitivity

Sensitivity, measured in coulombs/cm^2, is defined as the minimum electrical charge per unit area of resist film required for complete development of the exposed area (6). Its evaluation must include film thickness before and after development, electron energy developed image resolution developing time as well as the glass transition temperature, G values, molecular weight and molecular weight distribution of the polymer.

2. High Resolution

Resolution is indicated by the minimum line width that can be developed in a resist layer of a given thickness.

The resolution is adversely affected by electron scattering in the resist and in the substrate. This is termed as the 'proximity effect'. Other resist properties that affect resolution are contrast and swelling during development. The extent of swelling depends on the polymer structure, the molecular weight and glass transition temperature of the polymer and the nature of solvent. This is much more pronounced in case of the negative resists as compared to positive resists. Other factors such as resist thickness, beam accelerating voltage and exposure charge density must also be taken into account.

3. Adhesion to Substrate

This is required to minimize undercutting while maximizing edge acuity and feature size control. Poor adhesion can be detrimental to wet chemical etching and metallization processes that involve plating through a resist mask.

4. Etch Resistance

Resists should exhibit resistance to acidic and basic etching solutions employed in the silicon semiconductor industry. The etching solutions include buffered hydrofluoric acid for etching silicon dioxide, sodium hydroxide or a mixture of phosphoric and nitric acid solutions for aluminum etching, etc. Since undercutting will ultimately limit the resolution of liquid etching systems, the resist must also withstand dry etching techniques like plasma etching, ion milling, etc.

A high glass transition temperature is an important consideration for the dry etching of resists. During ion milling, the sample

undergoes a substantial temperature increase. If the resist does not have a high T_g, this temperature increase can cause it to flow affecting the resolution.

5. Low Defect Density

Pinhole formation can be avoided by using a high molecular weight polymer (7).

6. Resistance to Heating

A temperature increase is observed in additive metallization processes such as lift-off evaporation or sputter deposition. If the T_g is not high enough, the sample flows causing image distortion and preventing completion of the lift-off process.

The research for this thesis follows three principal directions to evaluate the resist characteristics of PMMA with the variation in the substrate, irradiation temperature and polymer structure.

In Chapter II, the current literature on PMMA based resists has been reviewed. The experimental techniques used in this study are outlined in Chapter III. The theoretical outlines for the temperature and substrate studies for PMMA are presented in Chapter IV. In Chapter V the results of these studies are discussed. Chapters VI and VII deal with studies on novel bromoacrylate and chloroacrylate systems respectively. The conclusions and suggestions for future work are given in Chapter VIII.

C H A P T E R II

REVIEW OF LITERATURE

So far PMMA has been the most frequently used positive resist. As mentioned earlier, the effects of the nature of the substrate, temperature and chemical modifications of the polymer structure on the G values have been of interest.

The substrates used in the industry include silicon wafers with or without silicon dioxide layers. It is possible that the G_S value for the polymer may be affected by the presence of the silicon dioxide layer. Therefore in our study, we have determined the G_S values for PMMA coated on to the two kinds of substrates. In silicon semiconductor devices the generation of "charge carriers" is accomplished by doping. This involves the addition of dopants like pentavalent phosphorus or trivalent boron to quadrivalent silicon. Since doped silicon wafers are employed in integrated circuit technology, it was decided to study the effect of doping the substrate on the G_S value of the polymer - PMMA in this case.

Various studies have been carried out regarding the effect of temperature on G_S on exposure of the polymer to γ radiation. Charlesby and Moore (8) found the G value for main chain scission to increase with temperature. The Franck-Rabinowitch cage effect is invoked to explain this temperature dependence. It was proposed that the reactive intermediates are held close together in the solid and may recombine. At higher temperatures the possibility of recombination is much lower due to diffusion. Therefore the probability of scission

becoming permanent increases at higher temperatures. Similar argument is presented by Boyer and Spencer (9), Wall and Brown (10) and Wundrich (11).

Charlesby and Moore obtained the activation energy from the Arrhenius plot to be 1.0 kcal/mole for a temperature range 0° to 180°C for both γ and electron radiation. Wundrich has reported an activation energy of 1.58 kcal/mole. They did not observe any discontinuity in the $\log_{10}$ G vs $1/T°(K^{-1})$ plot at the T_g or T_c. According to Wundrich, the activation energy changes near 0°C, the γ transition point. He found the activation energy below T_g to be 0.78 kcal/mole. Kroh and Polowinska (12) obtained the following activation energies for PMMA:

System/Temp.	Below -20°C kcal/mole	Above -20°C kcal/mole
PMMA deaerated	0.1	3.35
PMMA aerated	0.03	3.5

However their study was limited to temperatures between 0°C and -196°C.

Since these studies involved the γ irradiation of PMMA, a similar study was undertaken involving the exposure of PMMA to electron beam irradiation to see if the polymer behaved in a similar fashion.

PMMA has excellent resolution but has low sensitivity (5×10^{-5} coulombs/cm^2 at 15 kV) (13,14) and has a tendency to flow at elevated temperatures. It also displays poor resistance to various dry etching processes (13). Sensitivity of PMMA can be improved by introducing

chemical and steric configurations which tend to weaken the main chain stability of the polymer. This can be accomplished by introduction of bulky side group (15) or by substituting at the α position on the quaternary carbon atom with polar substituents (16).

Considerable work (16,17,18,19,20,21) has been done on the latter group of polymers involving substitution of fluorine and chlorine at the α positions and their G_S and G_X values have been evaluated. It has been reported that poly methyl α fluoroacrylate (PMFA) crosslinks even at low doses. However copolymers of MFA with MMA show a large increase in G_S values in comparison to PMMA.

In poly methyl α chloroacrylate (PMCA), scission takes place predominantly at doses below 6×10^{-4} C/cm^2 but a substantial increase in crosslinking is observed (19). G_S and G_X values were found to be 6.0 and $\sim 0.8 \pm 0.1$ respectively. High amount of crosslinking in those highly irradiated samples was attributed to dissociative electron capture of the C-Cl bond which is favorable for chlorine (17,22). Stronger C-F bond however renders dissociative electron capture exothermic for PMFA. As a result fluorine loss cannot be explained by this mechanism. However, the elimination of HF is possible (16).

In copolymers of MFA-MMA, chain scission is probably taking place due to the presence of MMA (16). The G_X value is not a linear function of the copolymer composition. For the copolymer containing small molar percentage of MFA, the G_X value is much more than expected. This suggests that if monomers whose polymers have high G_S as well as G_X values are copolymerized with monomers whose $G_X = 0$, e.g., MMA,

good positive resists may be obtained (16).

Lai and coworkers (18,23) found that there is a composition range in which the sensitivity of the MMA-MCA copolymer is substantially higher than that of either homopolymer. This effect has been attributed to a competing crosslinking reaction in homopolymers. They proposed that the rate of crosslinking associated with the comonomer is decreased in the copolymer because of random distribution of MCA units along the chain which reduces the probability of reaction of two MCA radicals which would lead to a crosslink. Rate of scission would be unaffected. Chen and Pittman (24) presented a similar argument for the MCA-MCN copolymers.

Pittman et al (25) reported that chlorine can be introduced to the ester without promoting crosslinking and have reported a G_S value of 2.7 and a zero G_X value for the homopolymer of trichloro ethyl methacrylate (TCEMA). However, Tada (26) found the homopolymer to show crosslinking behavior beyond 25 $\mu C/cm^2$. Lai et al (27) have further reported that the copolymers of TCEMA and MAN exhibit zero G_X values.

C H A P T E R III

EXPERIMENTAL

Sample Preparation

The polymers for these studies included PMMA obtained from duPont (Elvacite® 2041) and those prepared in the laboratory.

Synthesis of PMMA was carried out as follows. The monomer was vacuum distilled to remove the inhibitor. Required amounts of toluene and MMA-AIBN solution were charged in a pyrex glass tube, cooled and sealed in a vacuum system. Sealed tubes were placed in a constant temperature bath at 60 $\pm$ 0.1°C. After the requisite time, the contents of the tube were poured into excess of methanol and washed several times with methanol. Purification was carried out by repeated dissolution and precipitation from solutions in chloroform. Purified polymer was dried in vacuum to constant weight. Molecular weight was determined by GPC and tacticity by IR.

Copolymers of MMA with 2,3-dibromo methacrylate, methyl α bromoacrylate, methyl α chloroacrylate and trichloroethyl methacrylate were also prepared in the lab.

Their reactivity ratios were calculated by the Fineman-Ross method (28) and are listed in Table 1.

TABLE 1

Monomer Reactivity Ratios of MMA-Haloacrylate Copolymers

System	$r_1 \pm \Delta r_1$	$r_2 \pm \Delta r_2$
MMA-MBA	0.19 ± 0.02	0.16 ± 0.05
MMA-DBPMA	1.75 ± 0.13	0.82 ± 0.23
MMA-MCA	0.46 ± 0.1	0.13 ± 0.02
MMA-MTCA	0.28 ± 0.04	0.85 ± 0.12

Copolymers were prepared in bulk at 60°C using AIBN (0.1% by weight of monomers). Predetermined amounts of MMA, haloacrylate and AIBN were charged into a pyrex glass tube, cooled in liquid N_2 and sealed in high vacuum system. Sealed tubes were placed in a constant temperature bath at 60°C. Since the differential term of the copolymer equation was used, the conversion was limited to 10% in all cases. After the requisite time contents of the tube were poured into large excess of methanol and purified polymers were dried at 40°C under vacuum to constant weight. The composition of the polymers was determined by elemental analysis. The compositions and molecular weights of the polymers used in the evaluation of the G values are listed in Table 2.

Exposure Techniques

PMMA samples Elvacite 2041® and 3A (prepared in the lab) were dissolved in methyl ethyl ketone (MEK) to give solutions of 5% concentration by weight. Initially, chlorobenzene was chosen as solvent because it is the least volatile of solvents matching the solubility

Table 2

Molecular Weights and Compositions of Polymers Used in the Evaluation of the G Values

Polymer	m_2 mole %	$\overline{M}_n \times 10^{-5}$	$\overline{M}_n \times 10^{-5}$	$\overline{M}_w/\overline{M}_n$
PMMA-Elvacite 2021	0	2.20	4.62	2.1
PMMA (Prepd. in lab.)	0	3.71	5.08	1.37
P(MMA-MBA)	3	0.957	2.509	2.62
P(MMA-MBA)	5	0.403	0.907	2.25
P(MMA-DBPMA)	2	2.52	3.86	1.53
P(MMA-DBPMA)	5	does not dissovle in THF or $CHCl_3$		
P(MMA-MCA1)	15	2.814	3.447	1.22
P(MMA-MCA2)	20	2.492	4.024	1.61
P(MMA-MCA3)	42.5	2.110	3.385	1.60
P(MMA-MCA4)	61	1.450	2.490	1.71
P(MMA-MTC1)	9	3.019	4.321	1.43
P(MMA-MTC2)	24	2.192	3.197	1.45
P(MMA-MTC3)	35	1.696	2.634	1.55
P(MMA-MTC4)	38	1.321	2.115	1.60
PTCEMA	100	1.492	2.319	1.55

parameter of PMMA. This was replaced by MEK since the latter is less harmful to work with.

The wafers were cleaned thoroughly before coating. The wafer was spun on the Headway Model EC-101 spin coater and swabbed with cotton while spraying with clean MEK to remove any dirt. The coater holds the wafer in place by vacuum and spins at high speed (1000-5000 rpm). Cleaned wafers were weighed. Uniform films were obtained from polymer solutions by spin coating on to wafers.

Film thickness and uniformity depend on the viscosity of the resist solution, the spin speed and the evaporation rate. The resist solutions must be filtered carefully through 0.5 micron pore filter to minimize the defect density in the film due to particulate contamination.

Coating with extremely high molecular weight (> 600,000) polymer at high speeds should be avoided. At excess speed a fibrous layer is obtained. Spin times were 60 sec at an optimum spinning speed of 2000 rpm. This gave films about one micron thick. At higher speeds thicker films which did not cover the wafer completely were obtained.

For wafers coated with silicon dixoide, the oxide layer was removed from the bottom to ensure good conductivity in the exposure electron microscope. This prevents the occurence of the charging effect. This was done by etching for 10 minutes in a buffered HF solution of 40% NH_4F in H_2O and 48% HF in H_2O in a 9:1 mixture. During the etching process, the top SiO_2 surface was protected by coating with PMMA. After etching, the wafer was rinsed several times

with distilled water and the protective coating was removed with chloroform.

The coated wafers were prepared at 160°C under vacuum for 30 minutes (7,29). Coated wafers are usually prebaked at temperatures above the glass transition temperature (105°C) for sufficient time to remove stresses introduced during spinning. At high temperature, the polymer exhibits greater molecular mobility enabling strains generated during the coating process to be removed.

The ease with which the molecules move increases with the temperature. PMMA films must be heated to at least 160°C before the polymer is soft enough to allow solvent remaining in the film after the coating procedure to be released. Wafers were cooled after prebaking and weighed again. The thickness of the film can be calculated from its weight.

Electron Beam Exposure

A RCA Electron microscope was modified so that wafers of diameter 2" could be accommodated. We could not use smaller wafers since a large amount (2 mg) of the sample is required for Gel Permeation Chromatography. This microscope is shown schematically in Figure 1. Modifications involved the removal of the objective, intermediate and projective lenses, and the construction of a sample chamber large enough to accommodate a wafer of diameter 2". Accelerating voltages were changed from 50 keV and 100 keV to 22 and 44 keV respectively. A 3 mm aperture was placed just below the condenser lens pole piece to control the filament contour. Beam spread can be controlled by

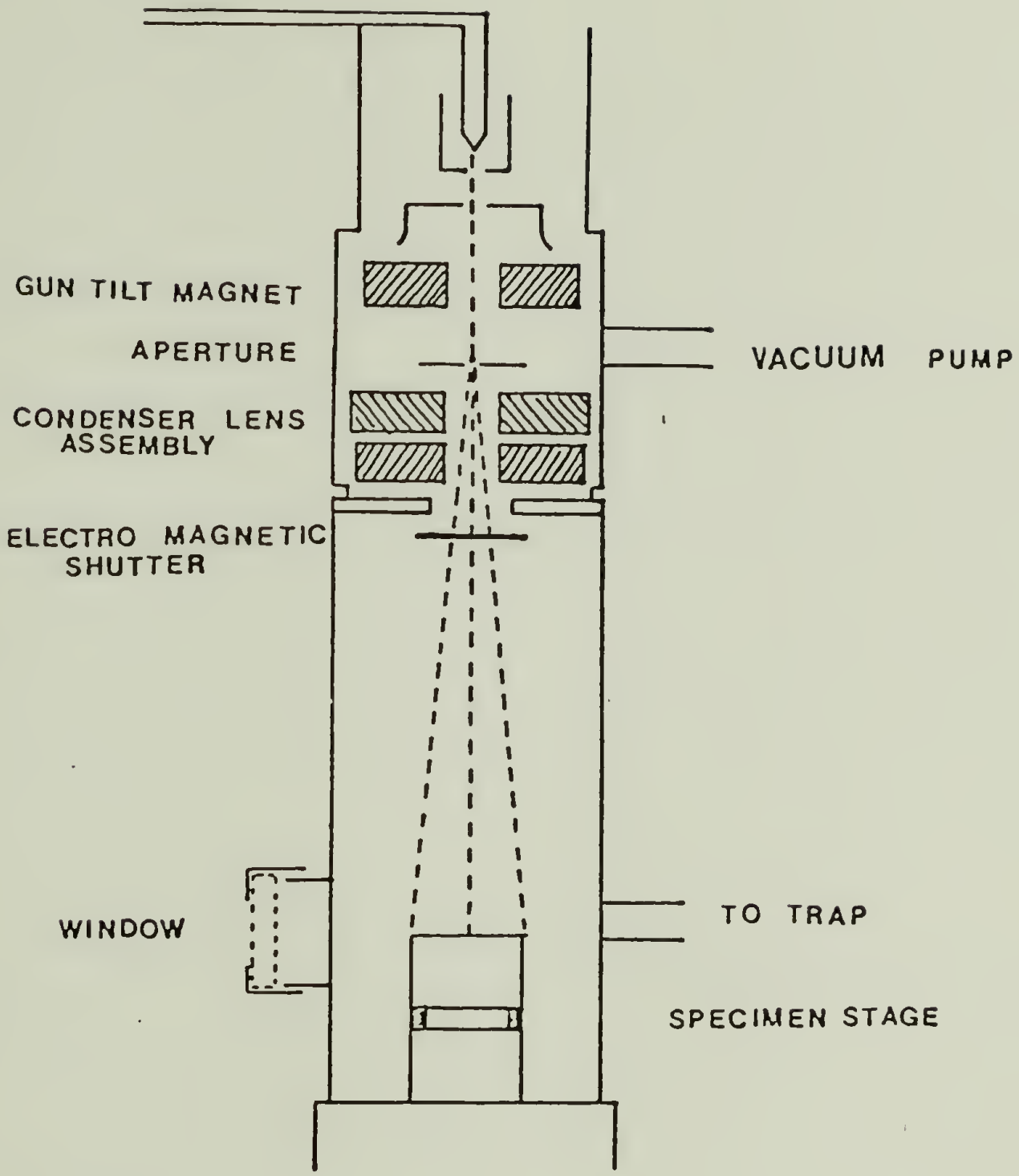

Figure 1. Schematic of modified RCA electron microscope.

adjusting the condenser lens current. Testing of beam homogeneity was done by putting a fluorescent screen on the stage and checking for any fluctuations.

The resist coated wafer is placed on the sample stage and the sample chamber evacuated to an operating pressure of approximately 10^{-5} torr. The beam current is monitored by a Faraday cup, placed at the stage periphery and connected to an ammeter. Exposure doses are controlled by a digital timer connected to an electromagnetic shutter mounted below the condenser lens. The exposure times in these experiments varied from 1 to 15 seconds. A chart recorder is used to record the ammeter output to take into account any beam fluctuations.

The exposed polymer film was removed from the wafer using chloroform, dried and then analysed by Gel Permeation Chromatography to determine the molecular weight.

Columns used in Waters Model 201 GPC ranged from 10^6 Å to 5 x 10^2 Å in size. Eluted material was detected by a differential refractometer relative to carrier solvent tetrahydrofuran (chloroform was used for analysis of chloroacrylate copolymers).

Polystyrene standards of molecular weight ranging from 10^3 to 10^6 were used to obtain a calibration curve of log M vs elution volume.

γ-Ray Exposure

Irradiation of some samples was carried out using a Cs 137 γ-ray source at room temperature. Calibration of the source was carried out by Fricke dosimetry as outlined in ASTM (30).

Fricke dosimetry is used for accurate measurement of the absorbed dose in water irradiated with γ rays. It is based on the process of oxidation of ferrous to ferric ions by ionizing radiation. The method can be used in the range from 0.2×10^4 rad to 4×10^4 rad, using spectrophotometric measurement of the ferric ion concentration.

Change in absorbance (at 305 nm) of an irradiated solution of ferrous ammonium sulfate is measured and the absobed dose calculated from that (31). Samples of the copolymers in pyrex tubes were evacuated at pressures of about 10^{-5} mm Hg for 20 hrs and sealed, after which they were irradiated. The dose rates varied from 0.07 to 0.03 Mrad/hr, depending on the total dose required. The highest dose applied was 1.5 Mrad.

Characterization Techniques Employed

The molecular weights and molecular weight distributions of the polymers were obtained by Gel Permeation Chromatography as mentioned before. The radical yield per 100 eV radiation absorbed G_{rad} was obtained from a double integration of spectra recorded on a Varian model e-9 EPR spectrophotometer.

Thermogravimetric analysis of the copolymers was carried out to measure the weight loss of sample and to observe its behaviour during thermal decomposition. DuPont 1090 TGA was used for the purpose. A heating rate of 20°C/min was used. T_g of the copolymers was measured by DSC using a Perkin Elmer DSC 2.

C H A P T E R IV

THEORY AND CALCULATIONS

In high resolution lithography, the interaction and scattering of electrons within the resist layer and the underlying substrate must be well understood. Various factors such as beam energy, type of resist, resist thickness and substrate type are critical in producing an optimal pattern in the resist (32).

Usual geometry employed in the exposure of a resist film on substrate is shown in Figure 2 (33). A well collimated beam of radiation is incident normally upon a resist film of thickness z = i, where only a small amount of reflection occurs at the top surface. The beam then penetrates the resist, where both scattering and absorption can occur. At the resist-substrate interface some of the radiation is backscattered resulting in additional absorption in the resist.

The resist-radiation interaction can be described in terms of the depth dose function which relates the rate of energy dissipation to the penetration depth into the film.

$$D(z) = I(z)t$$

$D(z)$ = Dose at penetration z

$I(z)$ = Electron intensity at z

t = Exposure time

Depth dose function for electrons is an empirical quantity based on measurement of ionization as function of beam penetration or on

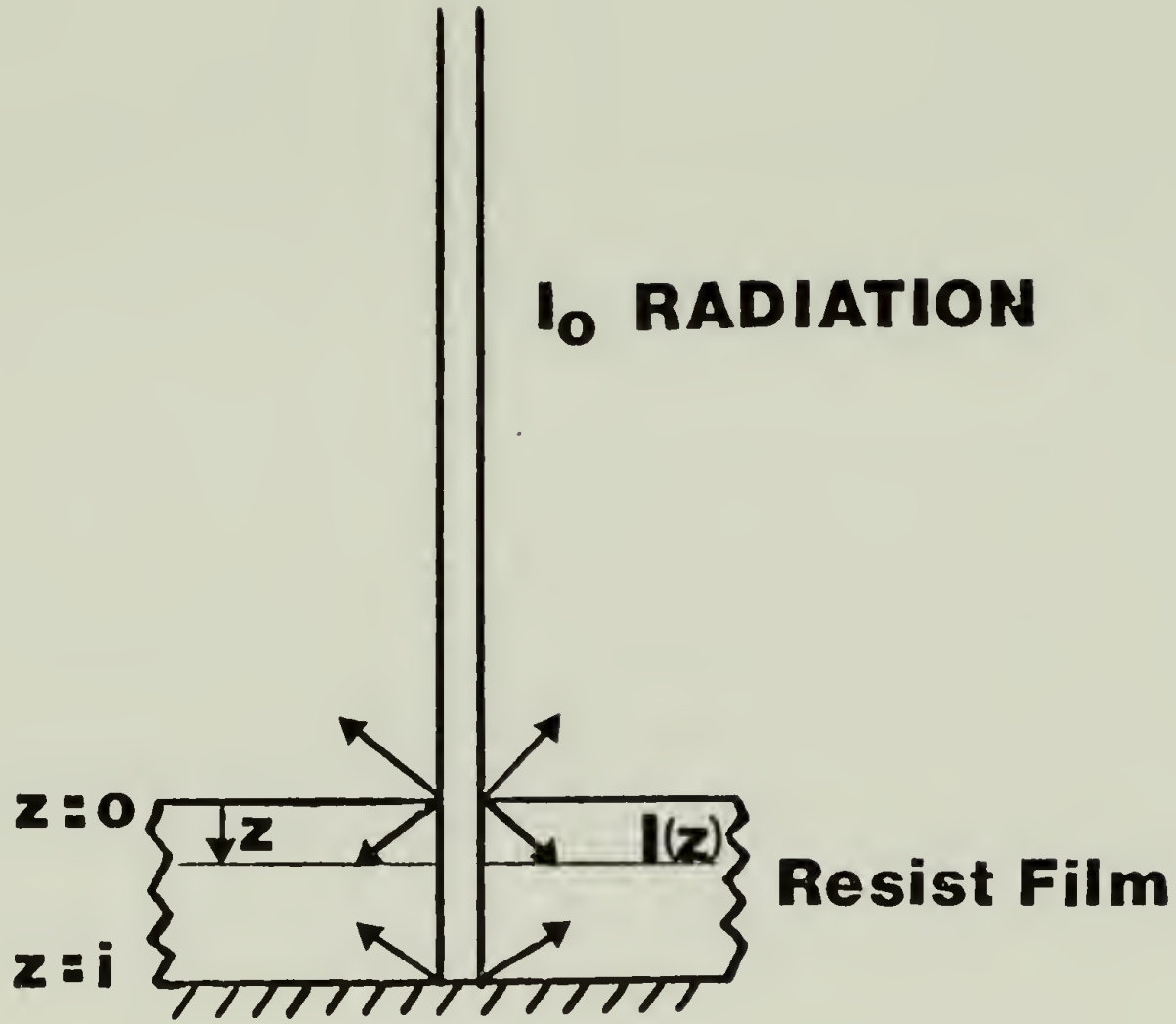

Figure 2. Collimated beam of radiation incident on a resist film of thickness i and scattered from the substrate. The incident intensity is I_o and I(z) is the intensity in the resist at penetration z.

measurements of penetration of incident electrons as a function of accelerating potential.

Extrapolation of various types of measurements leads to electron ranges R such as Grun range R_G, Bethe Range R_B etc. Range associated with extrapolated specific energy loss dE/dz to E = 0 is the Grun Range R_G.

$$R_G = kV_a^n$$

k = proportionality constant, V_a = accelerating potential, n = exponential

here $6 < Z < 15$ and $2 < V_a < 25$ keV

Z = atomic number

normalized penetration $f = z/R_G$

z = penetration depth

R_G is a function of accelerating potential V_a = 22 keV for our case

$$R_G = (0.046/\rho)V_a^{1.75}\ \mu m$$

$$= (0.046/1.2)22^{1.75}\ \mu m$$

$$= 8.566\ \mu m$$

where ρ = density in g/cm^3.

Empirically the normalized depth dose function $\Lambda(f)$ is expressed as a polynomial of the form:

$$\Lambda(f) = 0.74 + 4.7f - 8.9f^2 + 3.5f^3 \qquad (1)$$

Specific energy dissipation is then

$$\frac{dE}{df} = -V_a\ \Lambda(f) \qquad (2)$$

or

$$\frac{dE}{dz} = \frac{-V_a}{R_G} \Lambda(f) \qquad (3)$$

The normalized depth dose function $\Lambda(f)$ and the normalized kinetic energy $\Lambda(f)/V_a$ are plotted vs. the normalized penetration f. This relation determines the rate at which energy is transferred to the interacting solid as a function of penetration per incident electron.

Electrons entering a solid material are scattered by interaction with the atoms comprising that material. In the forward direction, most of the electrons deviate from their original direction, thus broadening the incident beam (33). Some electrons may be backscattered to return to the resist surface and contribute to additional ionization in the resist (Fig. 3).

Scattering is dependent on the electron energy, the resist and substrate material and pattern geometry. Therefore, most of the energy not absorbed by the film, will be absorbed in the substrate. A fraction of this amount will be backscattered into the film. The back scattering coefficient for electrons at these energies has been assigned a value of 0.1 (34,35,36,37,38,39). Additionally, this back scattered intensity is assumed to be totally absorbed in the film. Thus the total energy absorbed is the sum of the energy dissipated by the electron on the first pass through the film and the energy absorbed due to backscattering.

Scission yield is designated G_S. No of scission events = $E \cdot G_S/100$. E = energy (in eV) lost by electron in passing through the polymer film. The reaction yield depends on the nature of the polymer

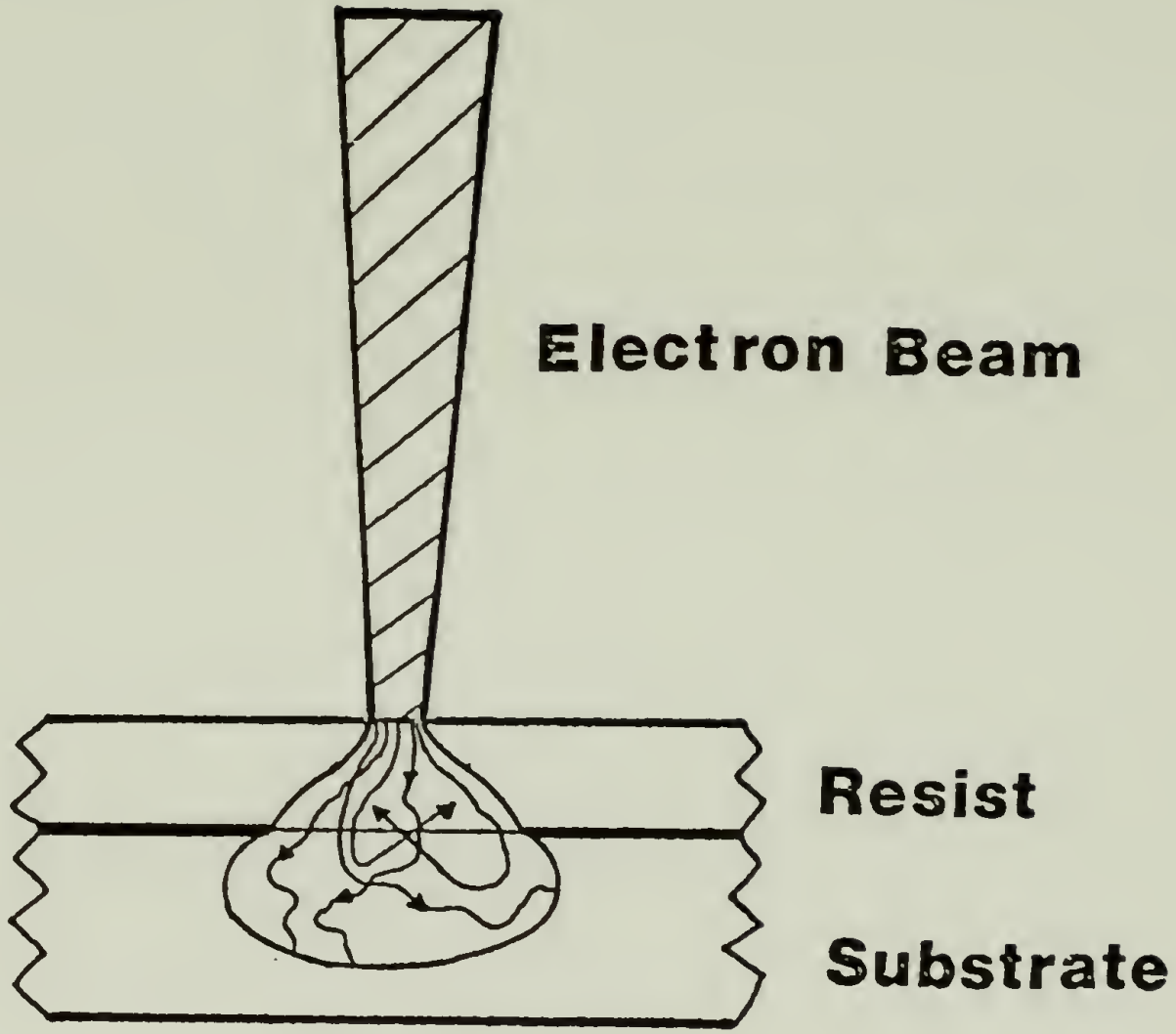

Fig. 3. Electron penetration and scattering effects in exposing a resist coated substrate.

and the bombarding radiation.

For electron energy of 10 keV or more and polymer films of thickness 1 micron or less, the energy loss may be considered to be uniformly distributed and the crosslinking or scission events are completely random (40).

The number of molecules, of molecular weight $\overline{M}_n$, in a polymer film of sheet density d gm/cm^2, are given by $Nd/\overline{M}_n$, where N is Avogadro's number.

The number of bonds in each molecule is given by $\overline{M_n}/(M_o^{-1})$ where M_o is the molecular weight of the monomer.

Thus the total number of bonds = $Nd/(1/M_o - 1/\overline{M}_n) \cong Nd/M_o$

For an electron dose of Q coul/cm^2, the number of scission events are = $QEG_s/100\ q$ where E is the total energy absorbed in ev. The probability of scission at a bond, P_s, is given by the expression:

$$P_s = QEG_sM_o/100\ qNd \qquad (4)$$

The number of bonds in each molecule of molecular weight $\overline{M}_n = \overline{M}_n/M_o$

Number of scission fragments = $P_s\ \overline{M}_n/M_o + 1$

Number average molecular weight of these fragments $\overline{M}_n'$ is given by the equation:

$$\overline{M}_n' = \overline{M}_n/(P_s\overline{M}_n/M_o + 1) \qquad (5)$$

$$1/\overline{M}_n' = P_s/M_o + 1/\overline{M}_n \qquad (6)$$

if $P_s\overline{M}_n/M_o >> 1$, then $\overline{M}_n' = M_o/P_s$ (7)

combining 4 and 7 we get

$$\overline{M}_n' = 100\ qNd/QEG_S \tag{8}$$

$$Q = 100\ qNd/EG_S\ \overline{M}_n' \tag{9}$$

eqn 5 can be rewritten as

$$1/\overline{M}_n' = QE(G_S - G_X)\ qNd\ 100 + 1/\overline{M}_n \tag{10}$$

An analogous equation for weight average molecular weight is given by Kilb (41).

$$1/\overline{M}_w' = QE(G_S - 4G_X)/qNd\ 200 + 1/\overline{M}_w \tag{11}$$

This equation is based on the following assumptions:

a) crosslinking and chain scission are random processes

b) G_S and G_X are independent of dose

c) Initial molecular weight distribution is random i.e., $\overline{M}_w = 2\overline{M}_n$.

Molecular weights necessary for analysis are obtained from GPC.

G_S and G_X values are evaluated from equations 7 and 8.

C H A P T E R V

RESULTS AND DISCUSSION OF PMMA STUDIES

In this chapter, the results of the substrate and temperature studies on PMMA are discussed. In this study, three types of substrates were employed. They were:

SD - silicon wafer with 5000 thick SiO_2 layer

SI - silicon wafer without SiO_2 layer

(SiO_2 layer < 100 Å in thickness)

SB - boron doped silicon wafer

PMMA used was Elvacite 2041. The experiments were carried out at room temperature.

$\overline{M}_n^{-1}$ vs. QE/qd N100 and $\overline{M}_w^{-1}$ vs. QE/qd N200 plots were constructed to evaluate the G_S and G_X values. These are shown in Figures 4, 5, 6, 7, 8 and 9. Results of the study are summarized in Table 3.

TABLE 3

Substrate Study of PMMA

	$G_S - G_X$	G_S	G_X
SD	2.139	2.371	0.232
SI	1.656	2.068	0.412
SB	1.779	1.916	0.137

The G_S values do not change substantially on using SI or SB wafers. There seems to be a slight increase in G_S on using the SD wafers.

A temperature study of PMMA was carried out next using boron doped

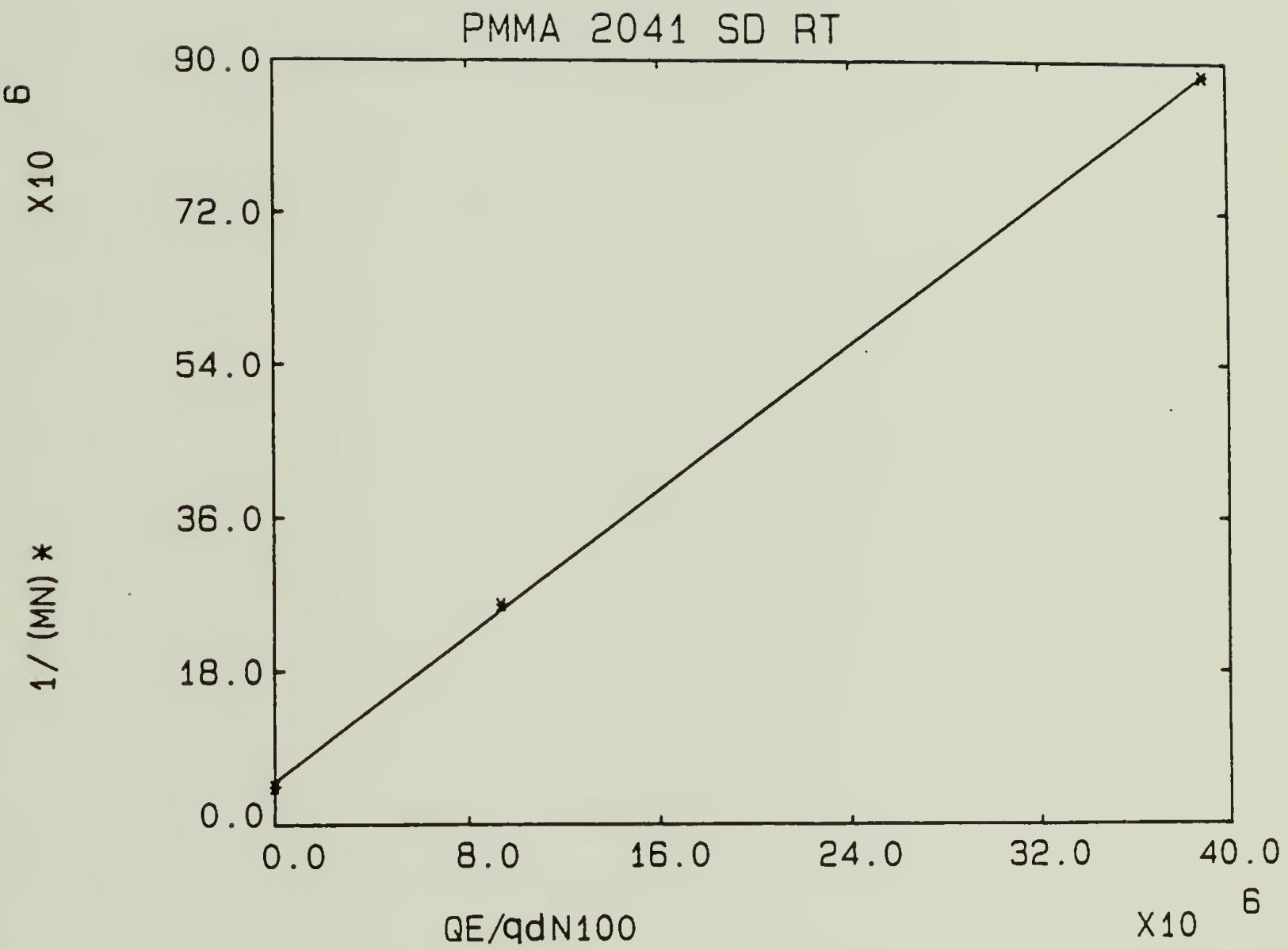

Figure 4. $1/(\overline{M}_n)^*$ vs. QE/qd N100 plot for PMMA coated on silicon wafer with 5000 Å SiO_2 layer at room temperature.

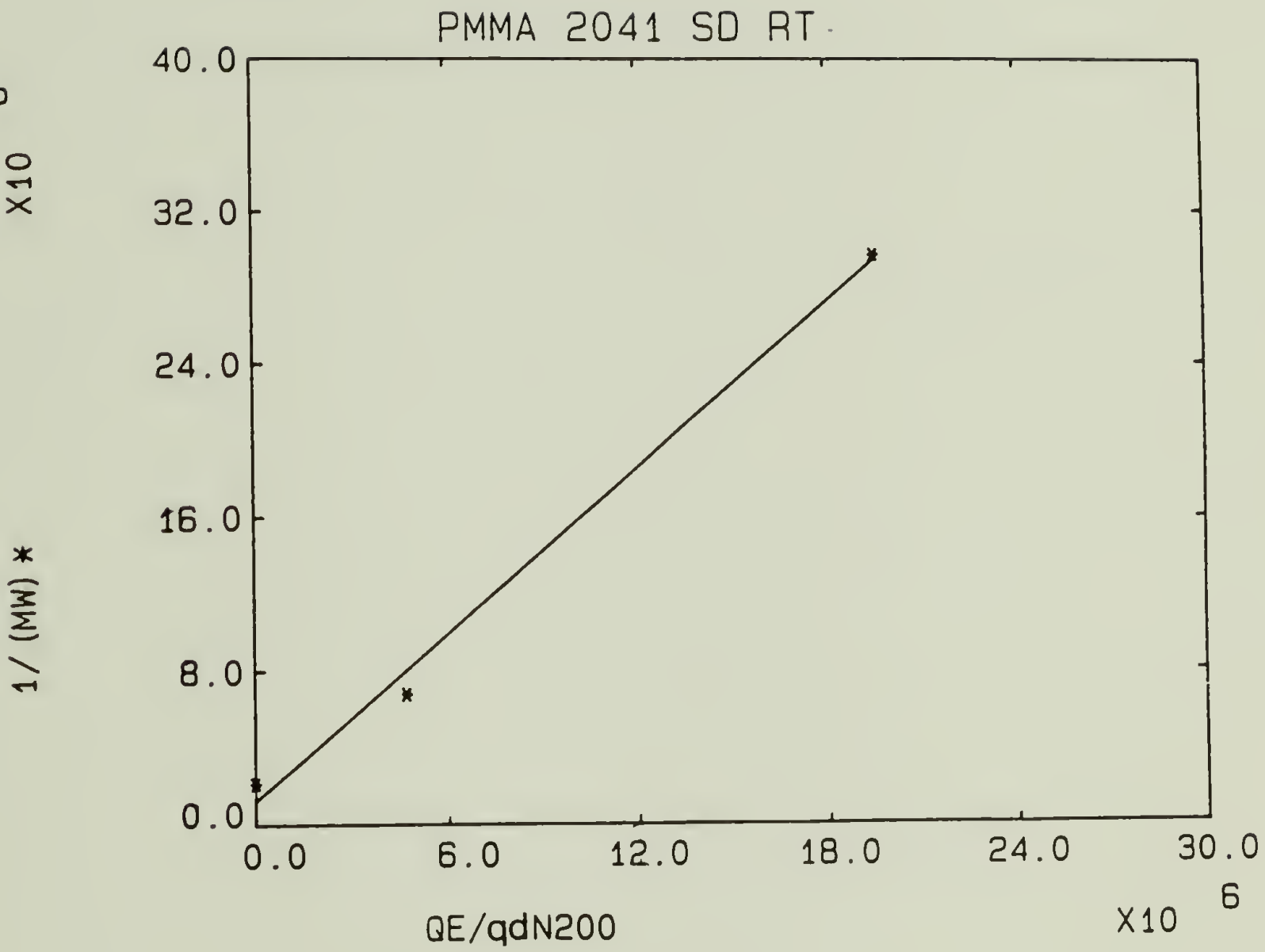

Figure 5. $1/(\overline{M}_w)^*$ vs. QE/qd N200 plot for PMMA coated on silicon wafer with 5000 Å SiO_2 layer at room temperature.

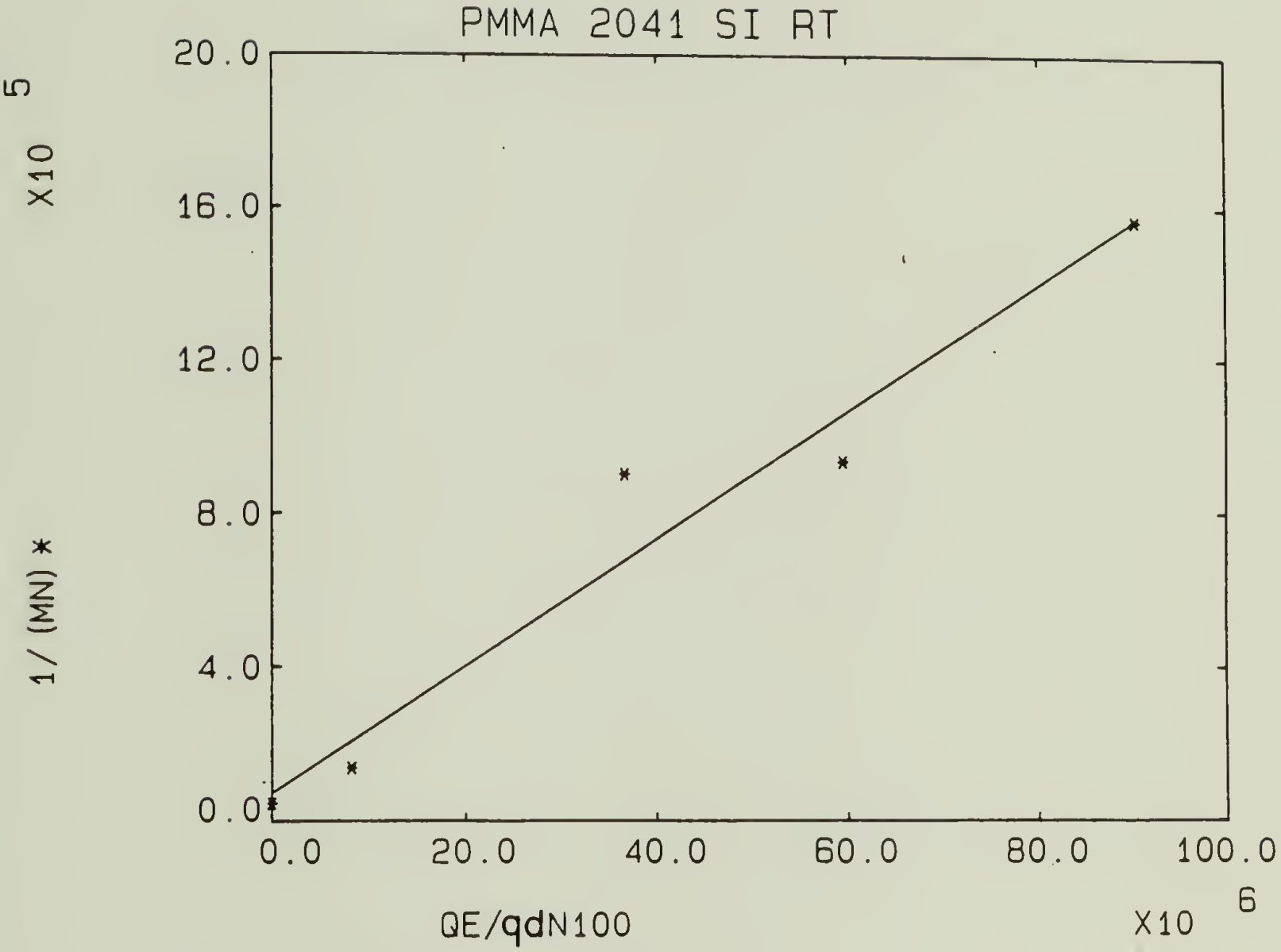

Figure 6. $1/(\bar{M}_n)^*$ vs. QE/qd N100 plot for PMMA coated on silicon wafer without SiO_2 layer at room temperature.

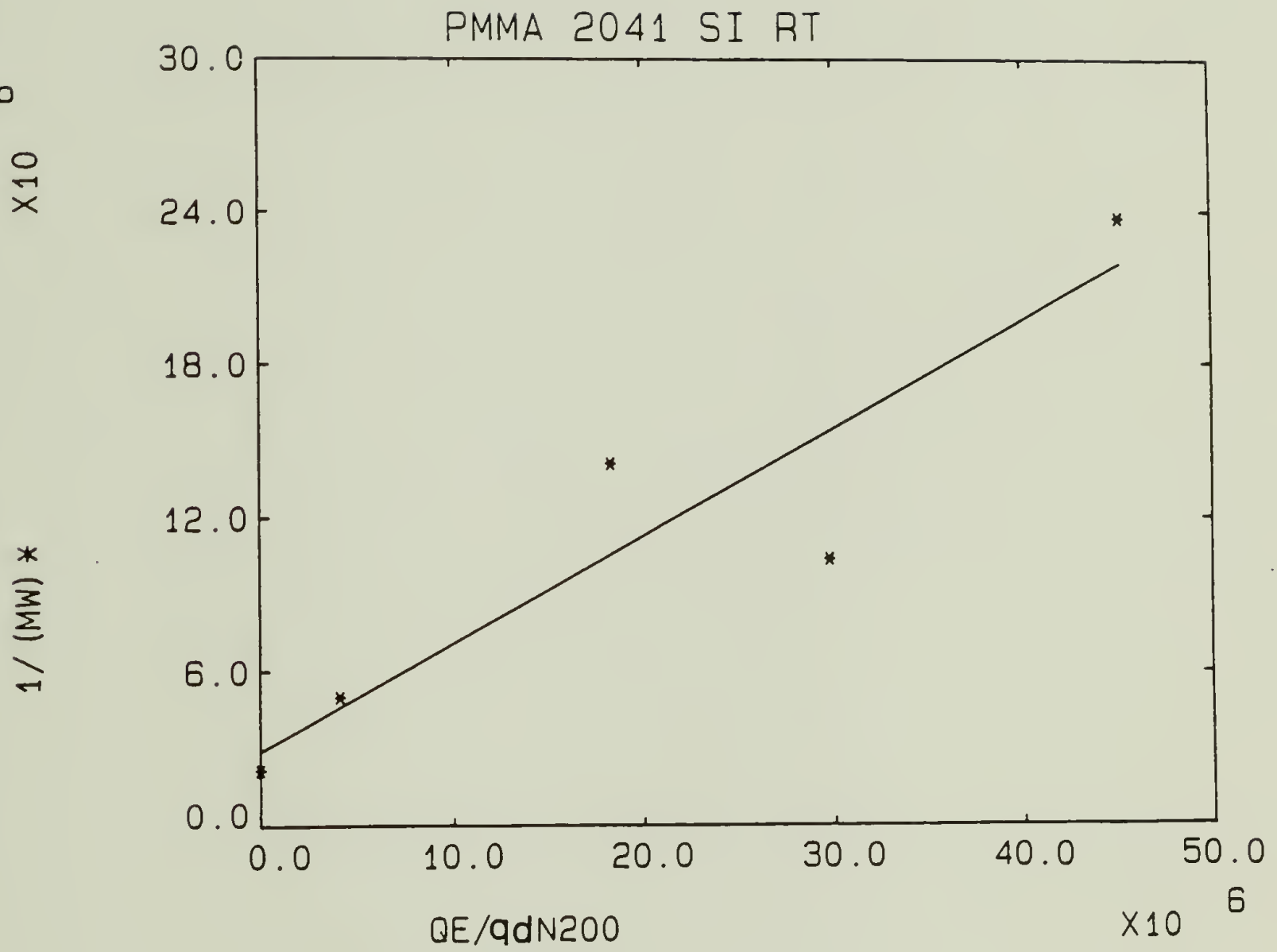

Figure 7. $1/(\bar{M}_w)^*$ vs. QE/qd N200 plot for PMMA coated on silicon wafer without SiO_2 layer at room temperature.

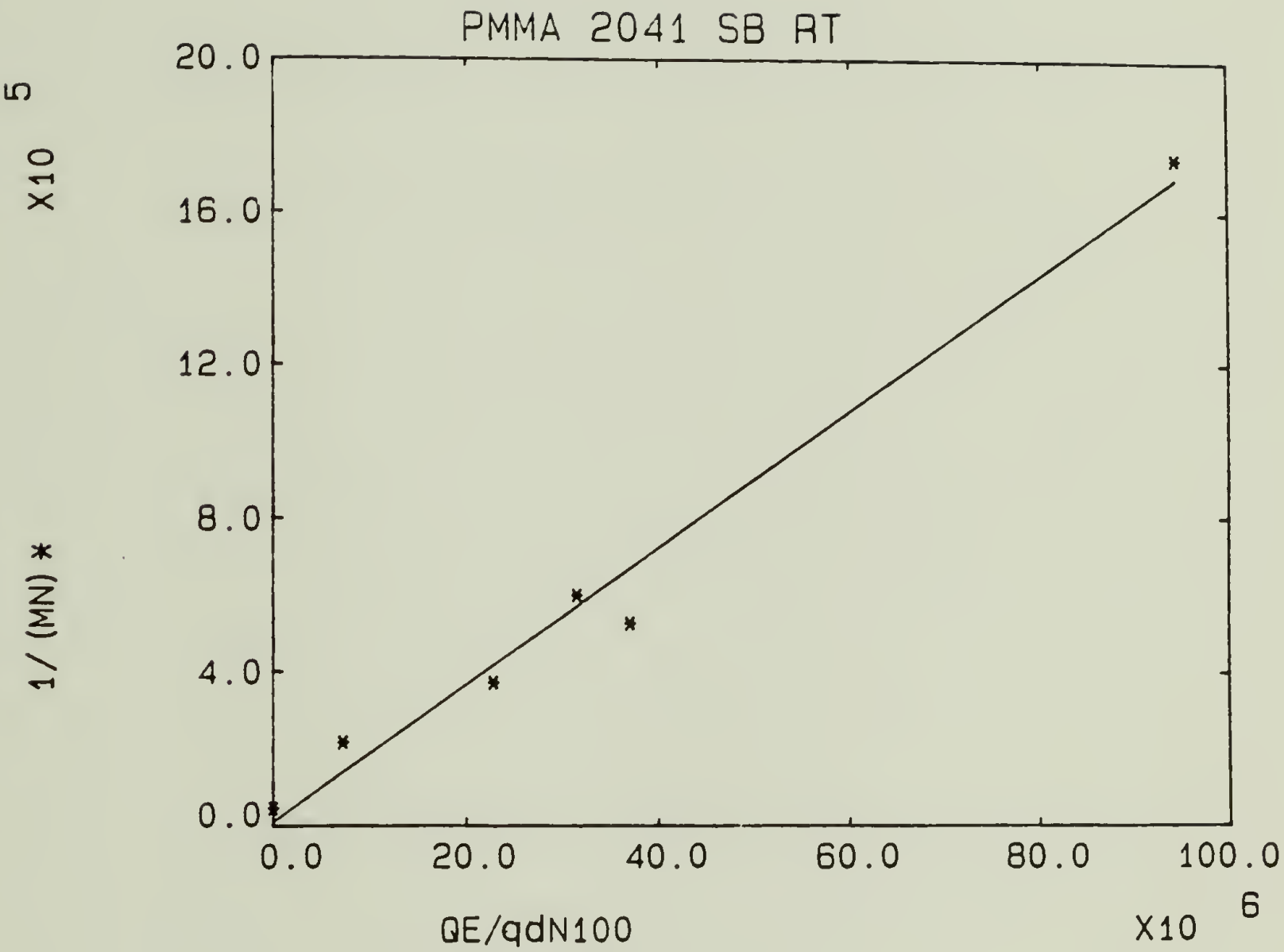

Figure 8. $1/(\overline{M}_n)^*$ vs. QE/qd N100 plot for PMMA coated on boron doped silicon wafer at room temperature.

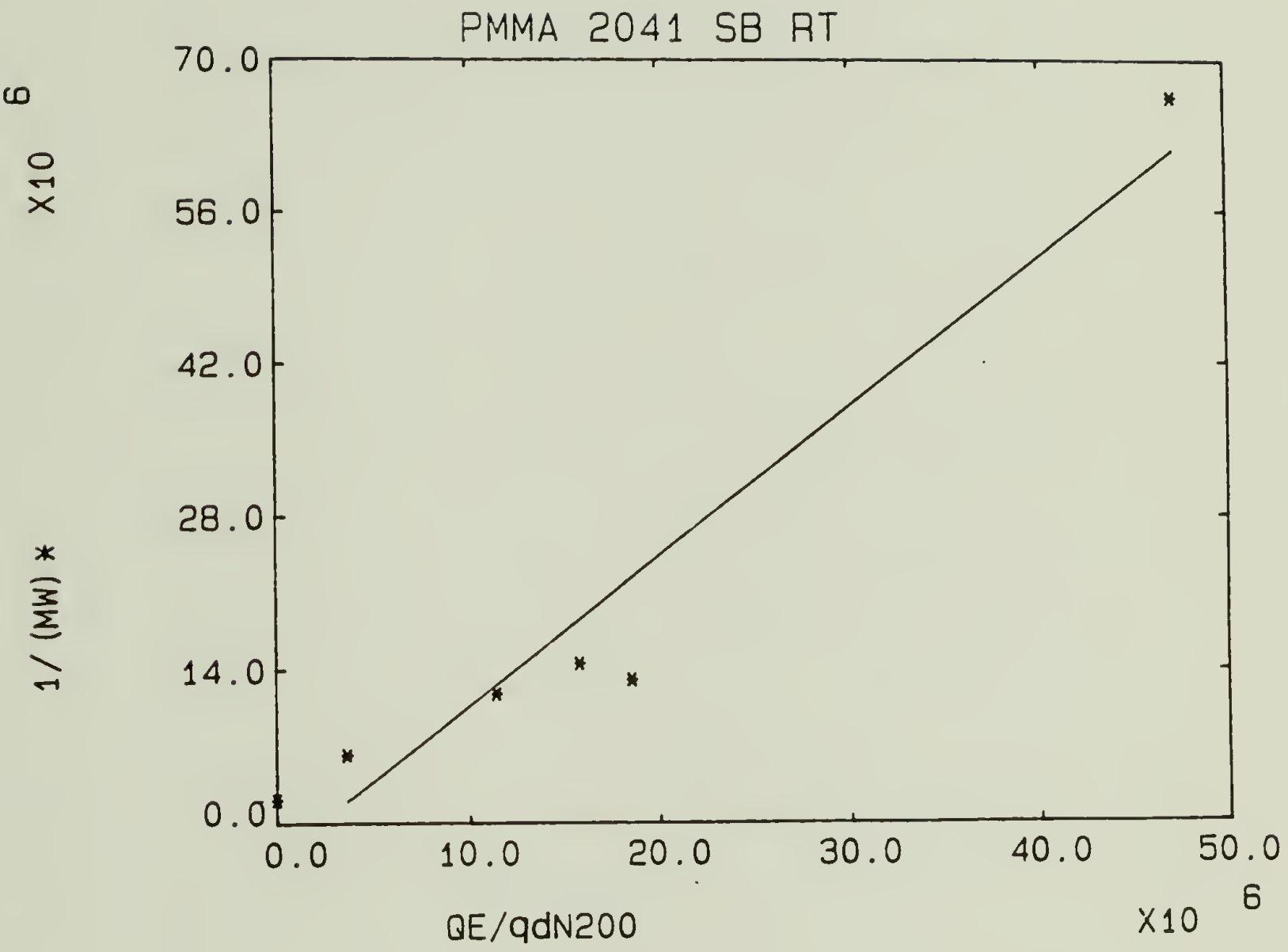

Figure 9. $1/(\overline{M}_w)^*$ vs. QE/qd N200 plot for PMMA coated on boron doped silicon wafer at room temperature.

silicon wafers as substrate. The polymer films were irradiated at room temperature, 80° and 160°C. $\overline{M}_n^{-1}$ vs. QE/qd N100 and $\overline{M}_w^{-1}$ vs QE/qd N200 plots were constructed as before to evaluate the G values. These are shown in Figures 10, 11, 12 and 13. A substantial increase in the G_S value was observed as function of increasing temperature. G values obtained are summarized in Table 4.

TABLE 4

Temperature Study of PMMA

Temp.	G_S-G_X	G_S	G_X
RT	1.779	1.916	0.137
20°C	4.355	4.728	0.373
160°C	10.722	10.05	0.67

To explain the temperature variation of G_S the Franck Rabinowitch cage effect is invoked according to which the reactive intermediates are held in close proximity in the solid and may recombine. At higher temperatures there is an increased probability of scission becoming permanent so that G_S tends to a maximum value equal to the number of excitations (and ionizations) per 100 eV.

Activation energy represents the minimum energy which the reacting molecules must possess over the average energy possessed by the ordinary molecule. A plot of $\log_{10}G(s)$ vs $1/T°(K^{-1})$ gives a straight line with a slope equal to $-E_a/2.303R$ from which activation energy E_a is obtained. This type of plot is termed an Arrhenius plot. An Arrhenius plot was constructed for the data obtained and the activa-

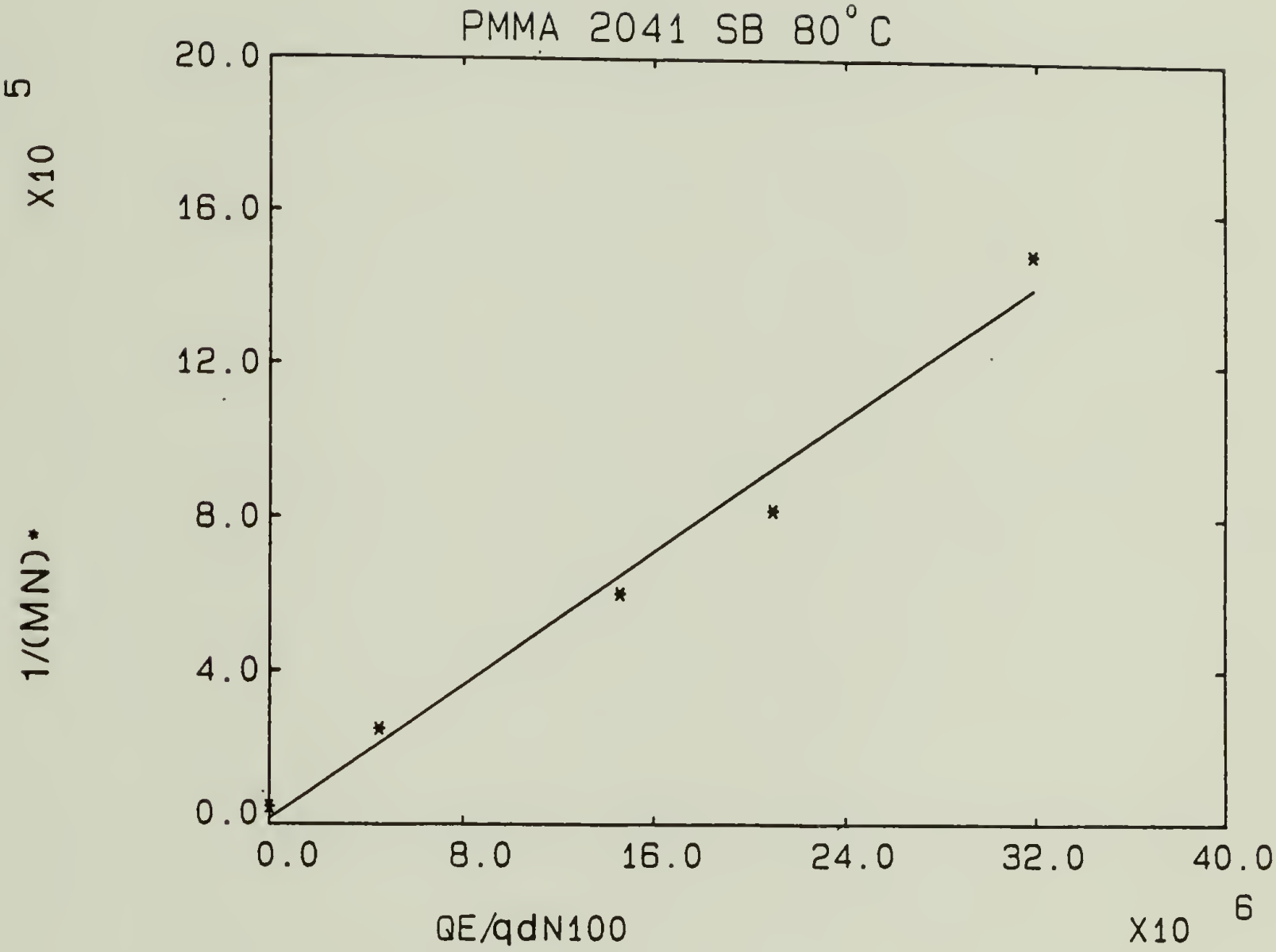

Figure 10. $1/(\bar{M}_n)^*$ vs. QE/qd N100 plot for PMMA coated on boron doped silicon wafer at 80°C.

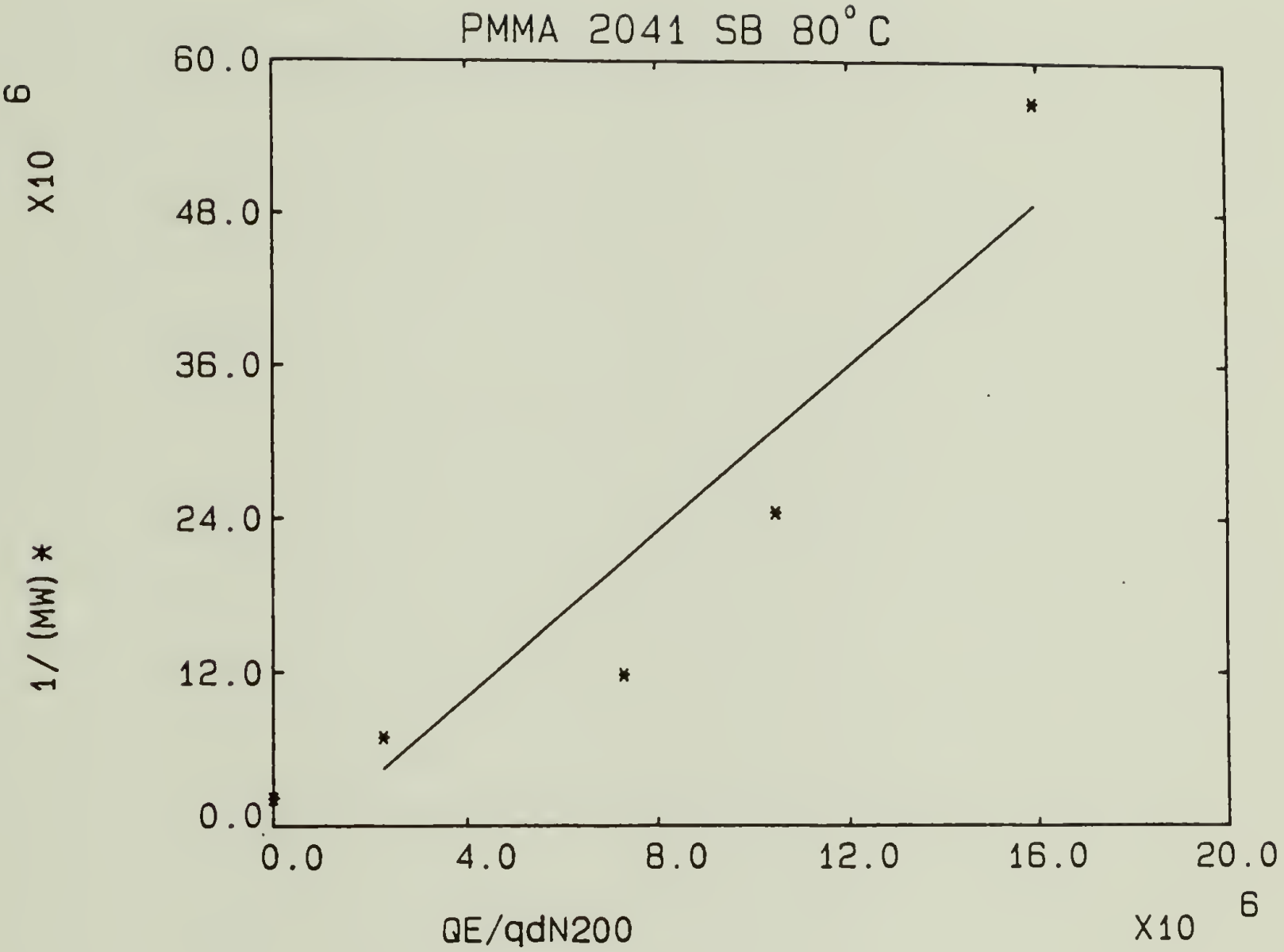

Figure 11. $1/(\overline{M}_w)^*$ vs. QE/qd N200 plot for PMMA coated on boron doped silicon wafer at 80°C.

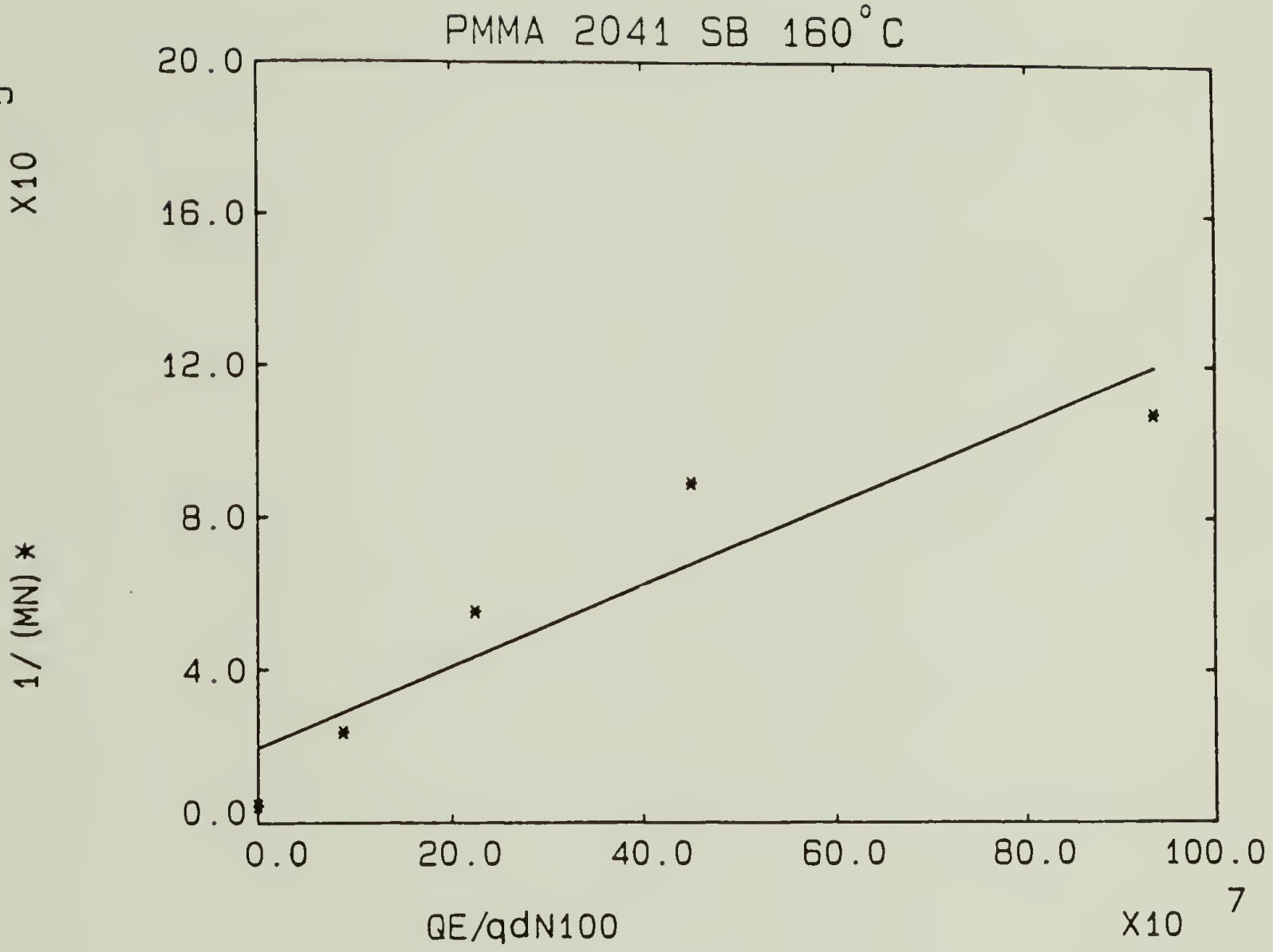

Figure 12. $1/(\overline{M}_n)^*$ vs. QE/qd N100 plot for PMMA coated on boron doped silicon wafer at 160°C.

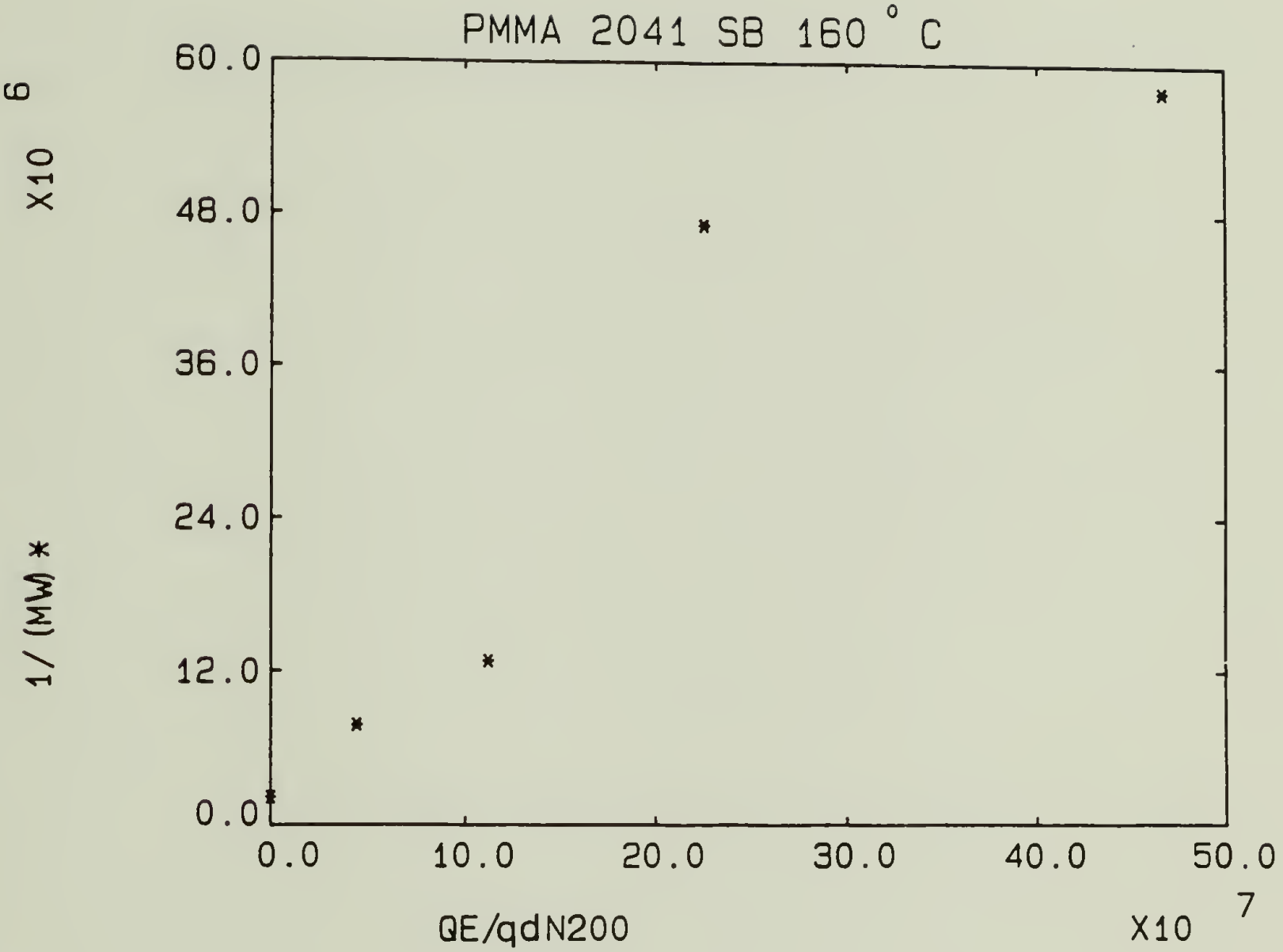

Figure 13. $1/(\bar{M}w)^*$ vs. QE/qd N200 plot for PMMA coated on boron doped silicon wafer at 160°C.

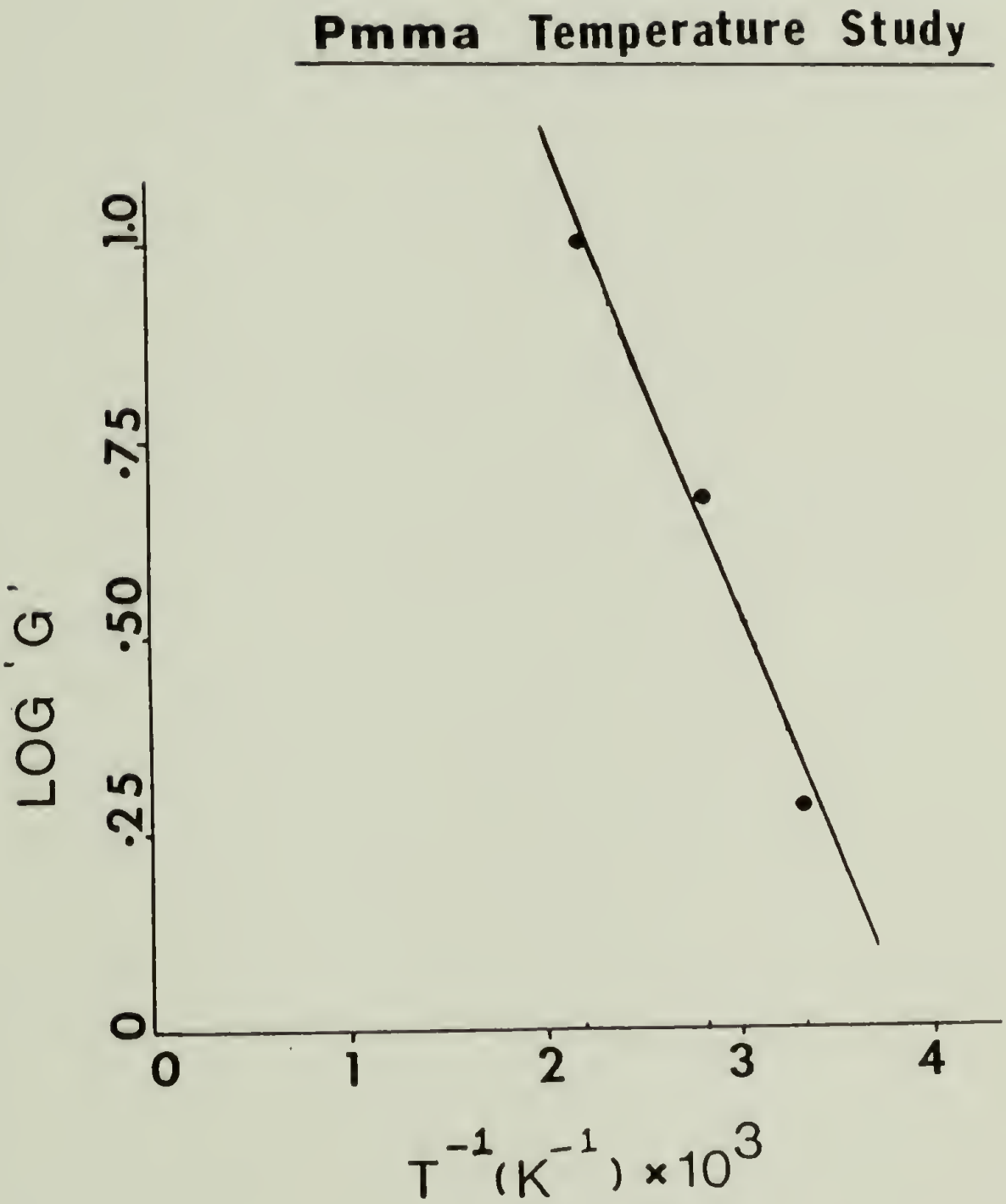

Figure 14. Arrhenius plot for PMMA.

tion energy was evaluated to be 2.78 kcal/mole. This is shown in Fig. 14. There is no discontinuity in the slope at the T_g or T_c. An important assumption is that E_a remains constant over this particular temperature range.

Charlesby and Moore (8) carried out a similar study using atactic PMMA (T_g = 105°C) in temperature range 0°C to 180°C. They obtained a constant activation energy of 1 kcal/mole for both γ and electron radiation. There was no discontinuity in the G value at the second order transition temperature at 57-68°C. Wundrich (11) obtained an activation energy of 1.58 kcal/mole for the scission process in PMMA on γ irradiation above T_γ = 5°C and 0.78 kcal/mole below T_γ. Charlesby and Moore exposed the samples to γ irradiation of intensities 0.1 and 0.5 Mrad/hr. Wundrich used γ radiation of intensity 1.5 Mrad/hr.

Kroh and Polowinska (12) plotted (1/M - 1/Mo) vs. $1/T(k^{-1})$ Arrhenius plots to obtain the activation energy. (1/M - 1/Mo) was taken to be proportional to the yield of degradation. M and Mo denote the molecular weight after and before degradation. Their results are summarized below.

System/Temp.	Below -20°C kcal/mole	Above -20°C kcal/mole
PMMA deareated	0.1	3.35
PMMA areated	0.03	3.5

Temperature range was 0° to -196°C.

They attributed the temperature effect to the changed conditions of radical deactivation i.e., to the lesser rigidity of the macro-radical structure and the larger mobility of the deactivating radicals.

Figure 15 shows the nine line spectrum of PMMA (42). In order to investigate the types of radicals present, power saturation was carried out. It was found that the four line splitting with a line width of 11 G saturates faster than the five line splitting. Similar observations were made by other workers (43,44).

Though there have been conflicting reports with regard to the observed splitting in PMMA majority of the workers (45,46,47,48) favor the nine line spectrum which arises from the propagating radical given below.

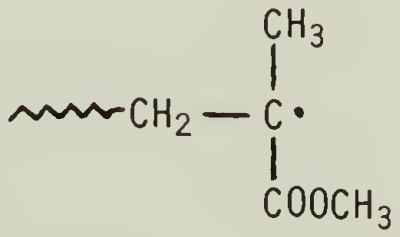

Effect of temperature on the concentration of radicals (i.e. G_{rad}) with temperature has also been studied - Fig. 16 and 17. The results indicate a substantial decrease in the concentration of radicals with an increase in temperature. There is an abrupt change in the radical concentration at 50°C which may be attributed to the faster decay of radicals due to the four line spectrum. At high temperatures, probability of the methylene protons preceding the propagating radicals would be higher and hence they both behave as a single proton with respect to the PMMA radical resulting in the predominant five line

Figure 15. EPR spectra of PMMA subjected to dose = 0.4 Mrad.

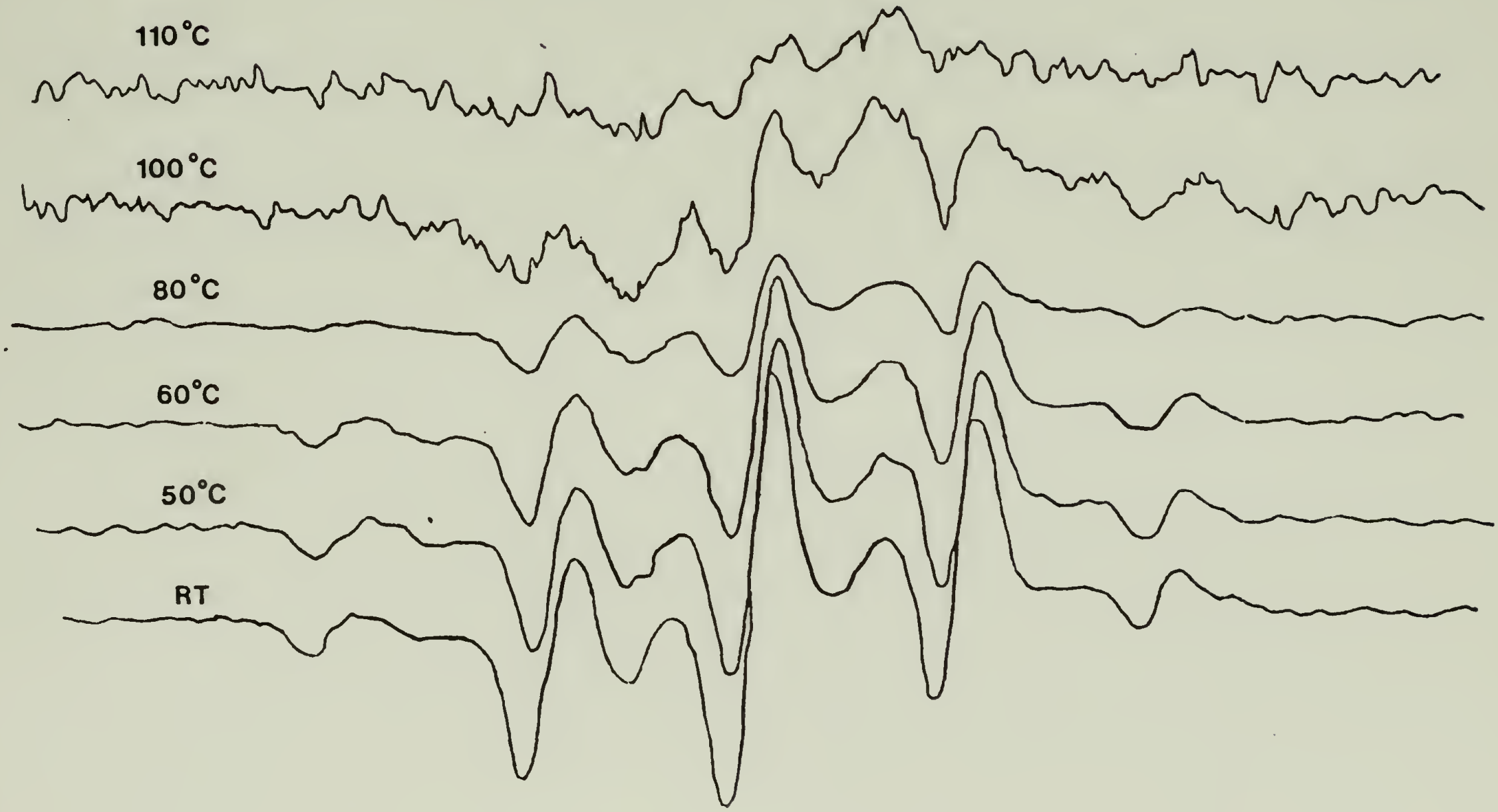

Figure 16. EPR spectra of irradiated PMMA as function of temperature.

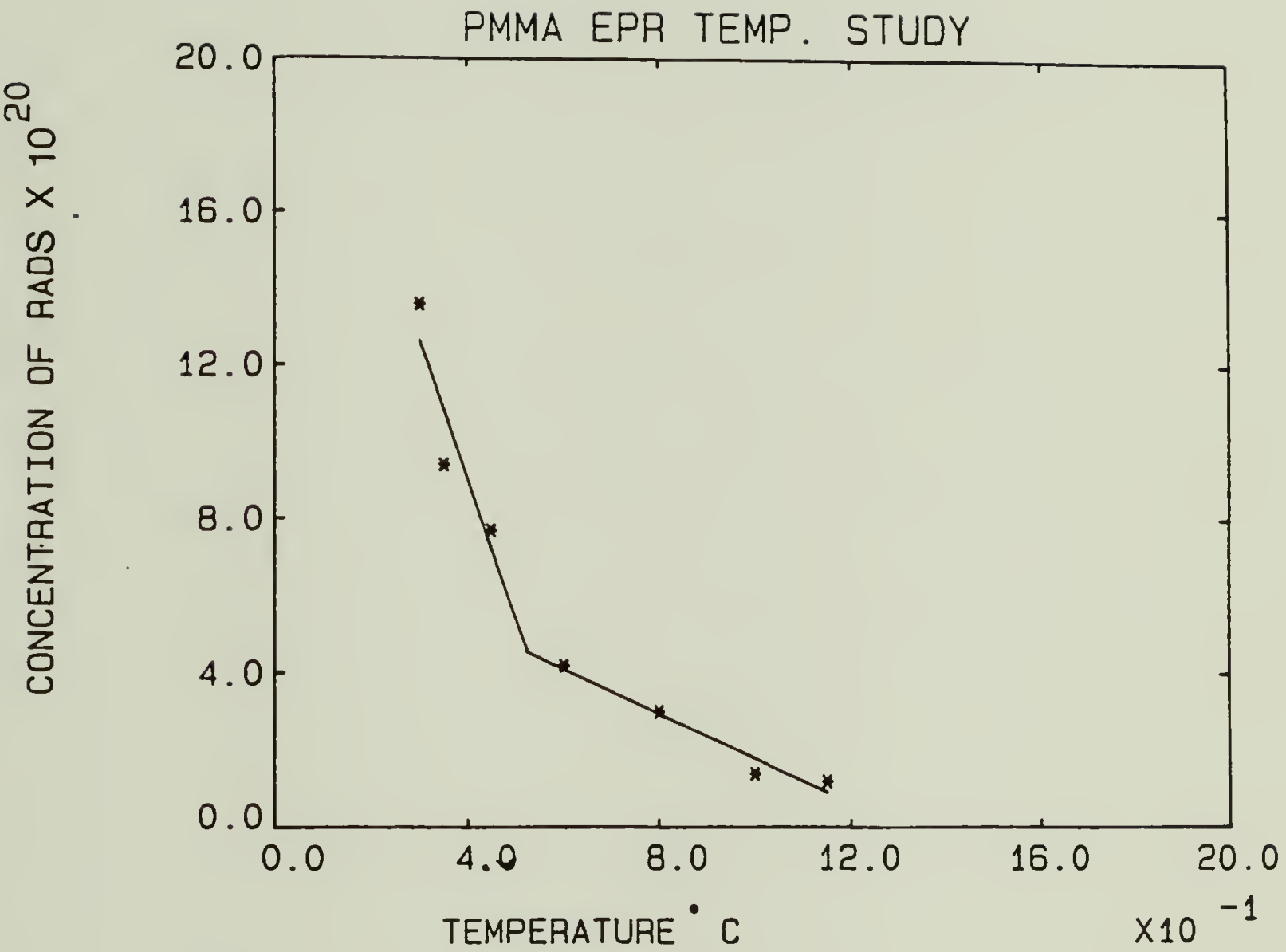

Figure 17. Temperature study of PMMA using EPR.

splitting. Further at 100°C the radical concentration totally disappears because of the mobility of the segments i.e., T_g of PMMA. This also indirectly confirms the T_g of PMMA.

C H A P T E R VI

BROMOACRYLATES

Introduction

It has been postulated that the sensitivity of PMMA can be improved by introducing chemical and steric configurations which tend to weaken the main chain stability of the polymer. This can be done in a number of ways (39).

According to Miller et al (49) crosslinking occurs if each segment contains one α hydrogen but degradation will predominate if the structure is:

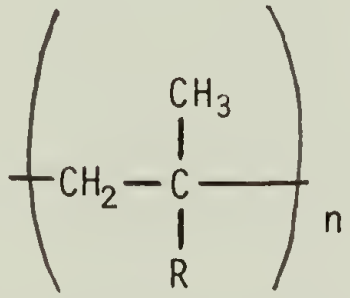

The lack of α hydrogen supresses crosslinking to some extent because free valency migration via hydrogen atom migration would be retarded. Structures of the above type, due to steric hindrance, have low heats of polymerization which have been correlated by Wall (50) to low gelling propensities. Scission probability can be increased by the introduction of a bulky side group or by substiuting at the α position on the quaternary carbon atom with polar substituents.

Results

Homopolymers and copolymers of methyl α bromoacrylate and 2,3-dibromo propyl methacrylate with methyl methacrylate were synthesized by procedures outlined in the experimental section. Monomer reactivity ratios were calculated by Fineman-Ross method (28).

TABLE 5

Monomer Reactivity Ratios of MMA - Bromoacrylate Copolymers

System	$r_1 \pm \Delta r_1$	$r_2 \pm \Delta r_2$
MMA-MBA	0.19 ± 0.02	0.16 ± 0.05
MMA-DBPMA	1.75 ± 0.13	0.82 ± 0.23

Both r_1 and r_2 values for P(MMA-MBA) system are less than one indicating the tendency towards alternating copolymerization. The preferential addition of MMA over MBA monomer to PMBA radical is attributed to steric factors due to the presence of bulky bromine vicinal to the propagating radical. The higher value of r_1 as compared to r_2 in the MMA-DBPMA system indicates the presence of relatively large blocks of MMA units interspersed with smaller DBPMA units.

The glass transition temperatures of MMA-MBA copolymers could not be determined. These polymers are probably undergoing post-polymerization reactions resulting in γ-butyrolactone rings along the polymer backbone. The glass transition temperatures of the 2,3-dibromo propyl methacrylate homopolymer and its copolymers with MMA are listed below in Table 6. These were less than that of PMMA and were found to decrease with an increase in DBPMA content. This decrease may be attributed to the decrease in intermolecular interactions of carbonyls due to bulky bromo alkyl pendant groups.

Copolymers have glass transitions at temperatures between those of pure homopolymers (51). Relation between the glass transition temperature and copolymer composition is given by:

$$1/T_g = W_1/T_{g_1} + W_2/T_{g_2} \qquad (12)$$

T_{g_1} and T_{g_2} are the glass transition temperatures in degrees kelvin of pure homopolymers 1 and 2. The corresponding weight fractions are W_1 and W_2.

TABLE 6

Glass Transition Temperatures of MMA-MBA Copolymers

System	m_2 mole%	T_g°C (observed)	T_g°C (calculated)
PDBPMA	100	53	
MMA-DBPMA	56.4	74	59.2
MMA-DBPMA	41.3	87	63.4
PMMA	0	104	

The heat stabilities of the copolymers were assessed using TGA. The thermograms of MMA-MBA copolymers showed two stage weight loss (Fig. 18). The TGA curves for poly(MMA-Co-MBA) depend upon the composition. The first stage weight loss decreases with the decrease of MBA content in the copolymer. This is interpreted as the elimination of CH_3Br from MBA units.

The TGA curves for the homopolymer of PDBPMA and poly(MMA-Co-DBPMA) show two distinct stages, an initial one at 200 - 225°C and complete pyrolysis at 360-460°C (Fig. 19). The latter is separated distinctly from the former for the homopolymer. The two processes merge into one another with an increase in temperature.

Table 7 gives the TGA data for MMA-methyl α bromoacrylate copolymers.

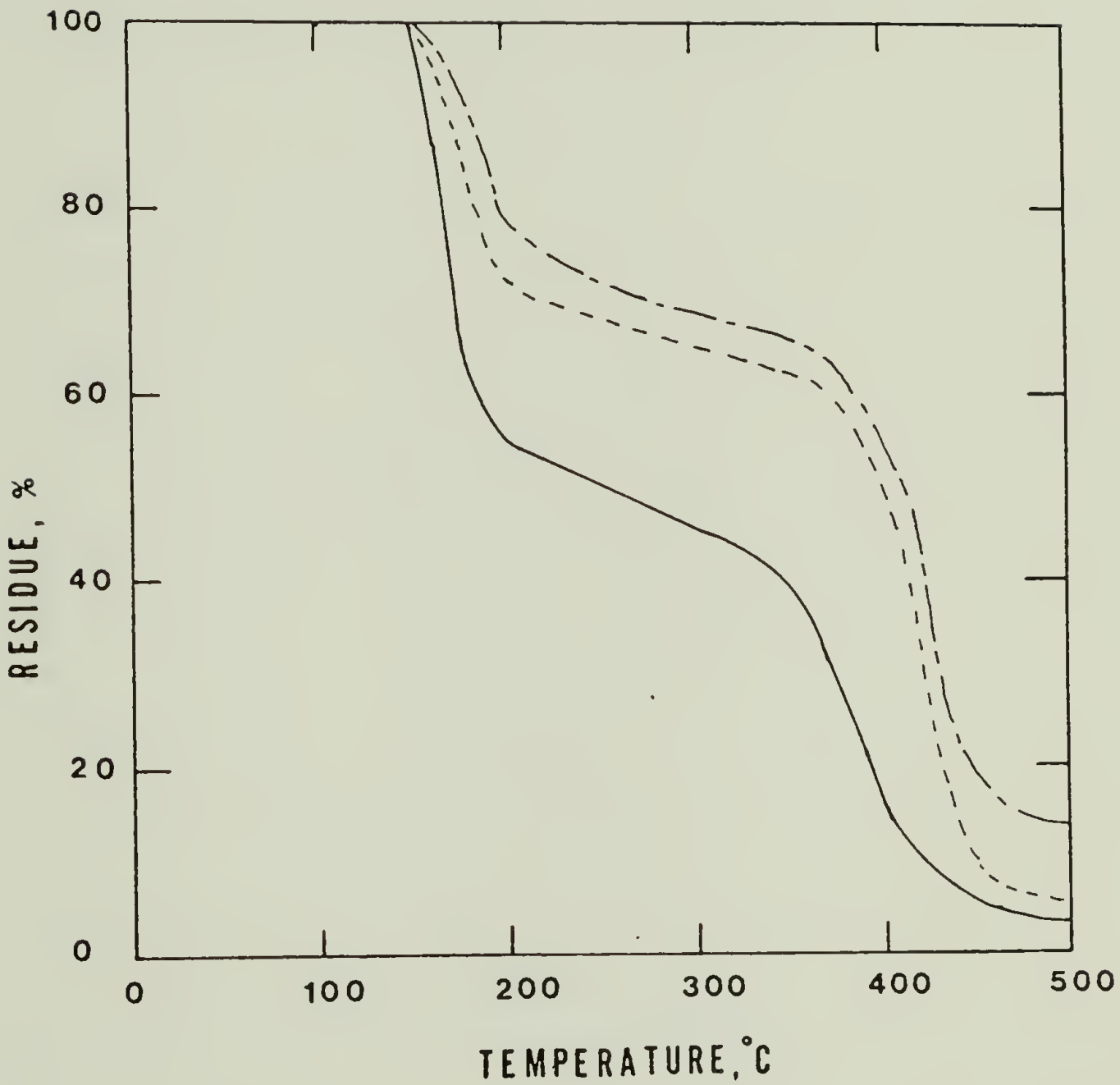

Figure 18. Thermogravimetric analysis of MMA-MBA copolymers (———) PMBA; (····) MMA (53) - MBA (47); (-·-·-·-) MMA (50) - MBA (50).

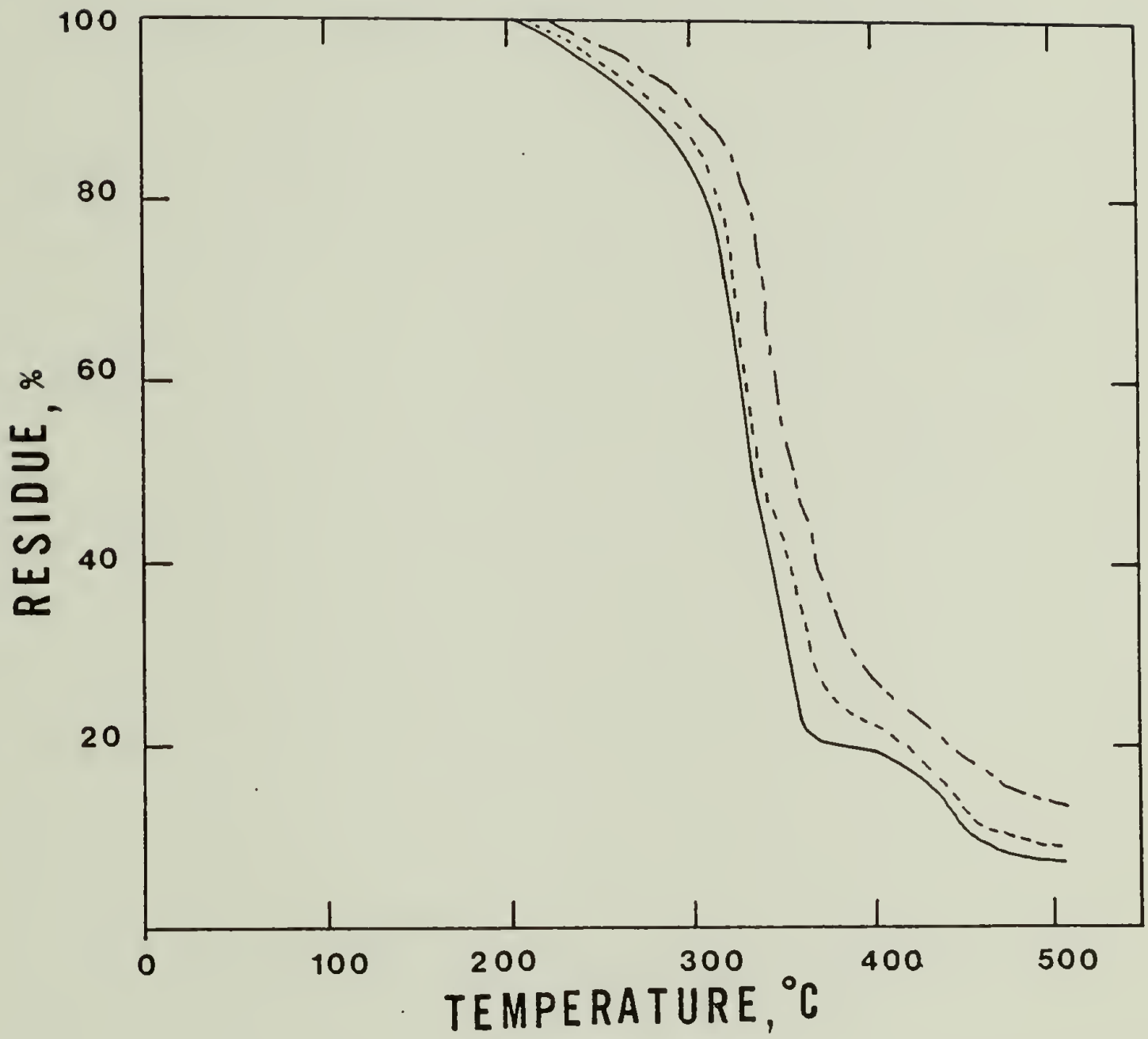

Figure 19. Thermogravimetric analysis of MMA-DBPMA copolymers (———) PDBPMA, (----) MMA (44) - DBPMA (56), (-·-·-·-) MMA (59) - DBPMA (41).

Table 7

TGA Data of MMA-MBA Copolymers

Polymer	m_2, mole % in copolymer	IDT[a]	weight loss at different temp.,°C		
			20%	40%	60%
PBMA	100	150	165	180	350
MMA - MBA	51	150	185	370	413
MMA - MBA	47	150	195	380	420
PDBPMA	100	200	307	324	340
MMA - DBPMA	56	200	310	327	350
MMA-DBPMA	41	200	330	345	367

[a]Initial decomposition temperature.

Table 8 gives the composition of MMA-MBA copolymers obtained from thermogravimetric and elemental analyses.

Table 8

Comparison of Composition of MMA-MBA Copolymers Obtained from Thermogravimetric and Elemental Analyses

Polymer	MBA composition from	
	TGA %	elemental analysis %
PBMA	98	100
MMA-MBA	38	40
MMA-MBA	49	49

A series of copolymers of varying compositions (Table 9) were used in the evaluation of G values.

TABLE 9

Molecular Weight and Compositions of Bromine Containing Vinyl Polymers for Degradation Studies

Polymer	m_2 mole %	$\bar{M}_n \times 10^{-5}$	$\bar{M}_w \times 10^{-5}$	$\bar{M}_w/\bar{M}_n$
P(MMA-MBA)	3	0.957	2.509	2.62
P(MMA-MBA)	5	0.403	0.907	2.25
P(MMA-DBPMA)	2	2.52	3.86	1.53
P(MMA-DBPMA)	5	Does not Dissolve in THF or $CHCl_3$		

These copolymers were irradiated to different doses and $\bar{M}_n^{-1}$ and $\bar{M}_w^{-1}$ vs. dose plots were constructed to evaluate G_S and G_X values (Fig. 20,21,22,23). All results are compared with PMMA which gave G_S = 1.4 and G_X = 0. G values of the systems studied are summarized in Table 10.

TABLE 10

G_{rad} at 298°k and G_S-G_X for γ Irradiated Bromine Containing Vinyl Polymers

Polymer	m_2-mole %	G_S-G_X	G_S	G_X	G_{rad}
PMMA	0	1.4	1.4	0	1.42
P(MMA-MBA)	100	-	-	-	6.98
P(MMA-MBA)	50	-	-	-	1.01
P(MMA-MBA)	7	-	-	-	2.33
P(MMA-MBA)	5	11.31	11.95	0.65	--
P(MMA-MBA)	3	5.8	5.34	0.46	2.01
P(MMA-DBPMA)	24	-	-	-	1.7
P(MMA-DBPMA)	5	3.47	3.62	0.14	--
P(MMA-DBPMA)	2	1.41	1.62	0.21	--

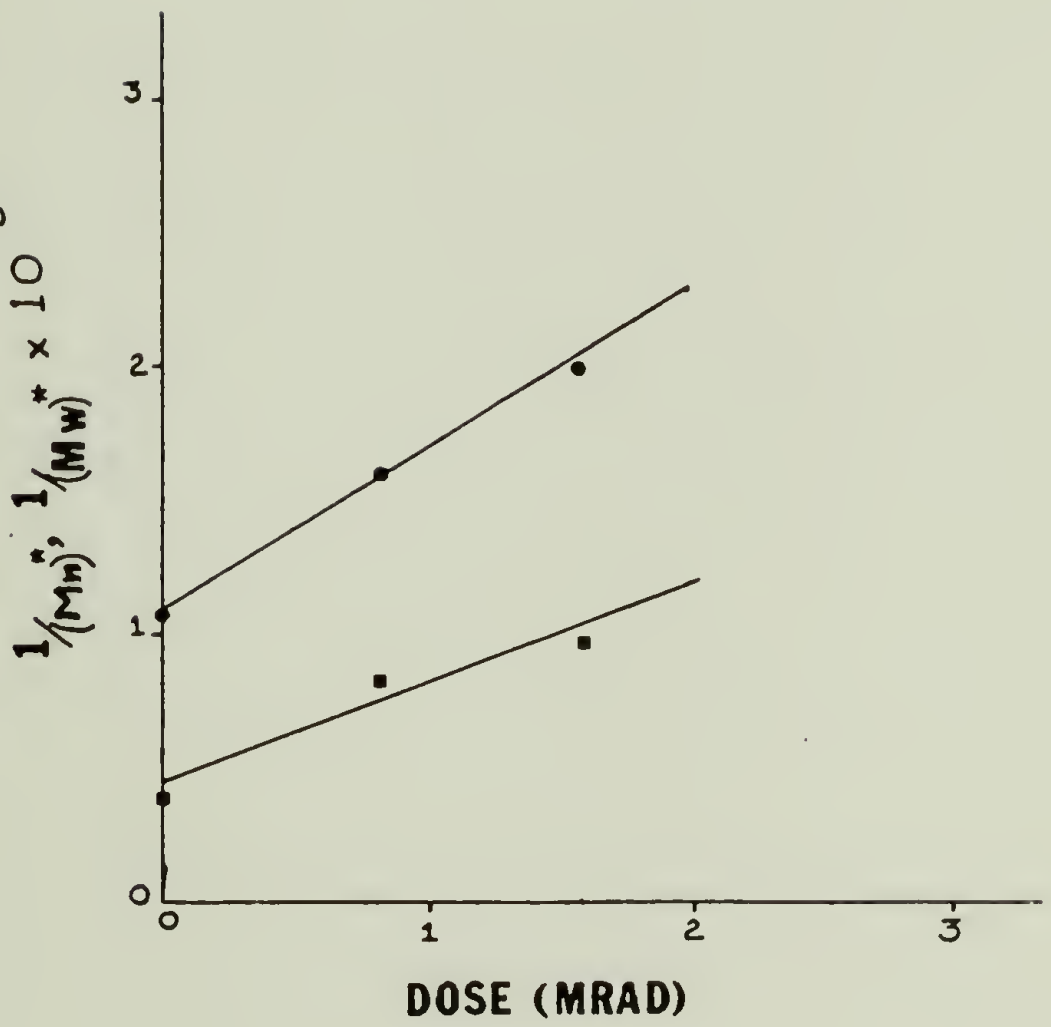

Figure 20. $1/\bar{M}_n)^*$, $1/(\bar{M}_w)^*$ vs. dose plot for (MMA-MBA) (97:3) copolymer.

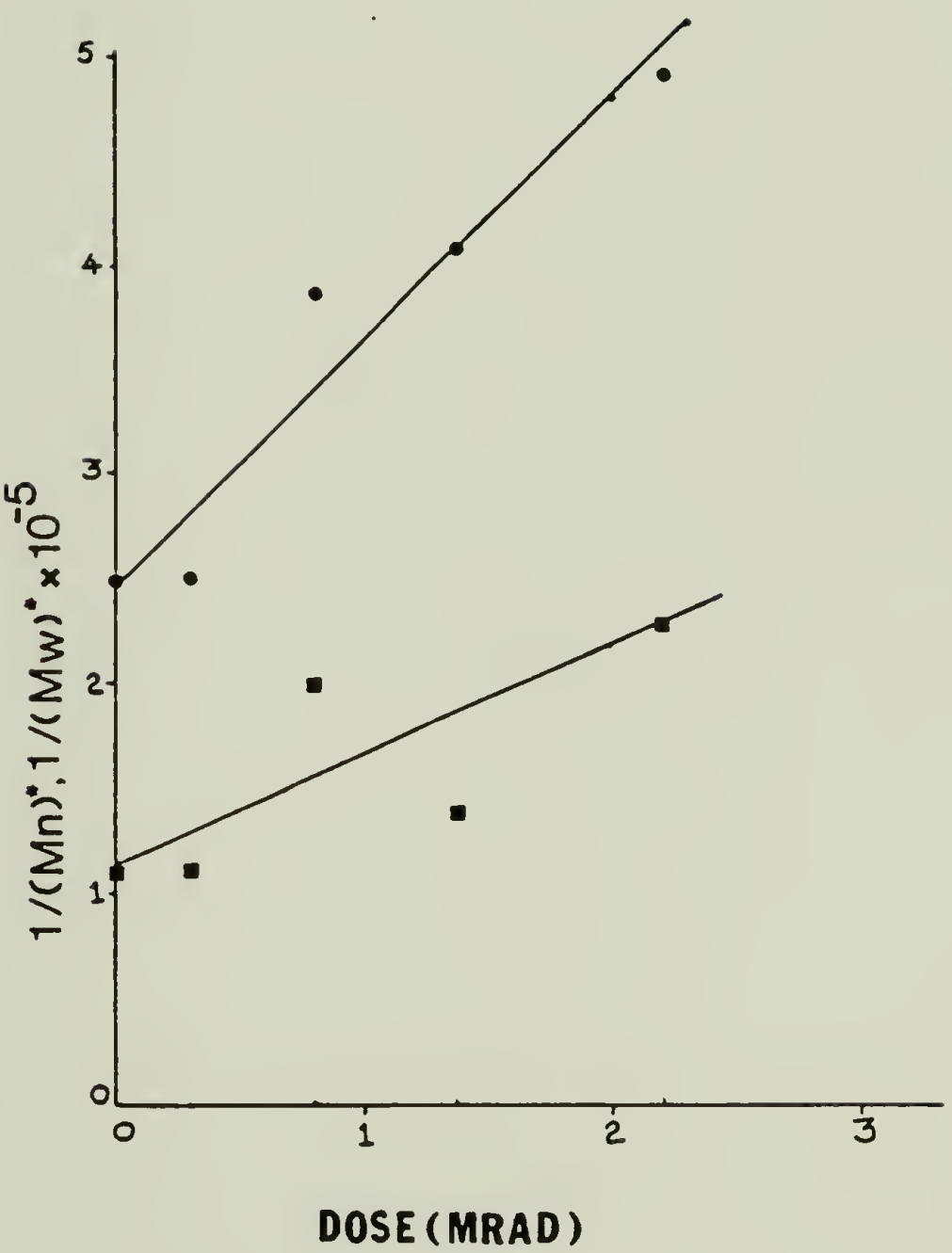

Figure 21. $1/(\overline{M}_n)^*$, $1/(\overline{M}_w)^*$ vs. dose plot for (MMA-MBA) (95:5) copolymer.

MMA-2MD

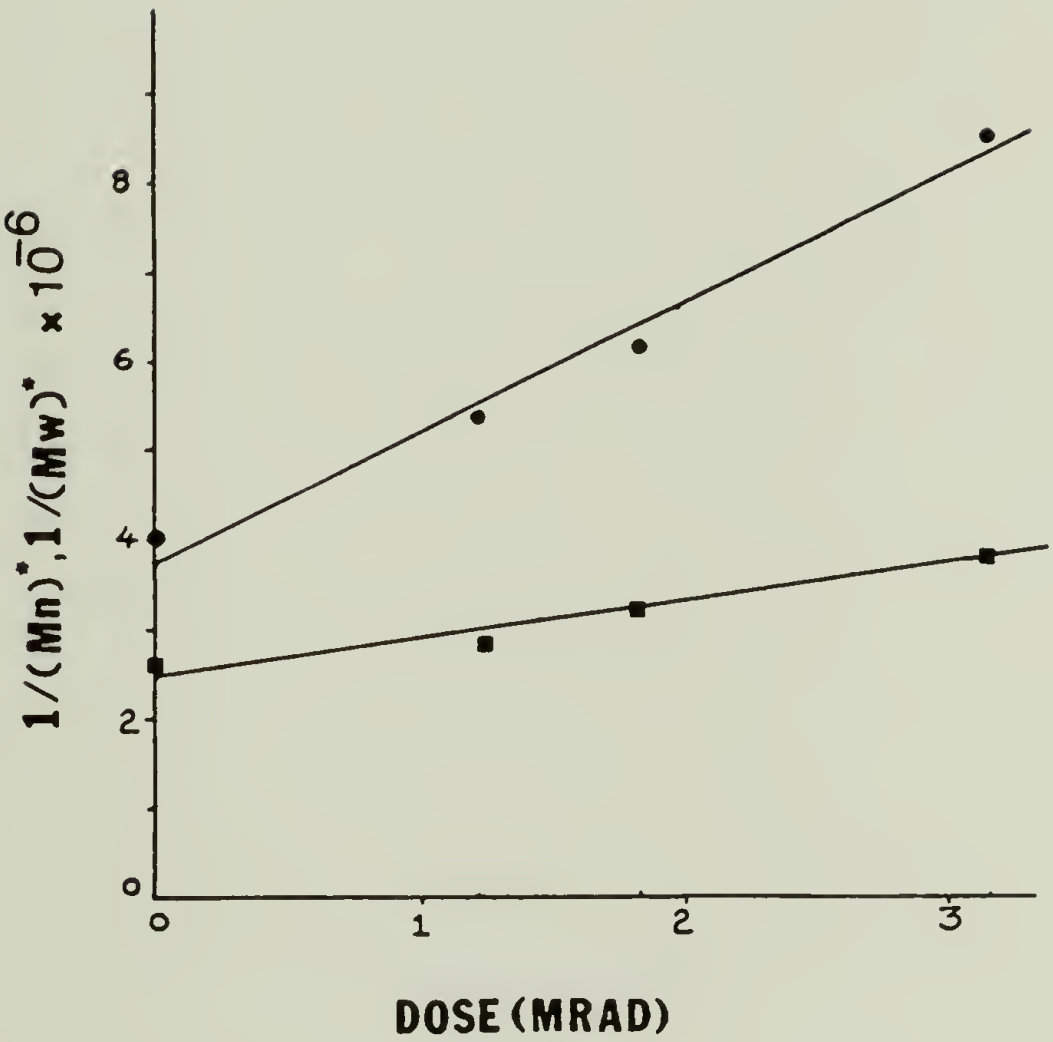

Figure 22. $1/(\overline{M}_n)^*$, $1/(\overline{M}_w)^*$ vs. dose plot for MMA-2MD copolymer.

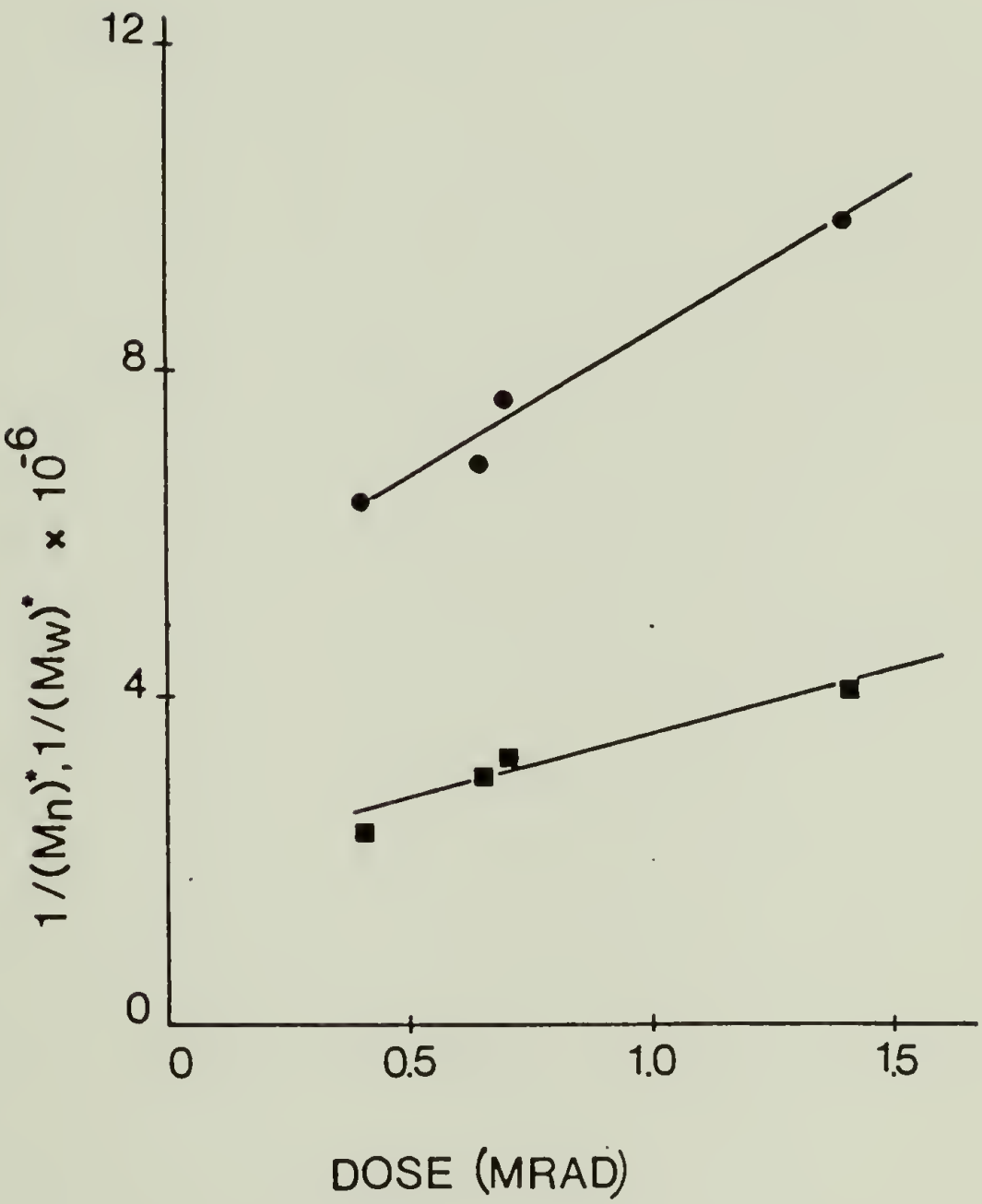

Figure 23. $1/(\bar{M}_n)^*$, $1/(\bar{M}_w)^*$ vs. dose plot for MMA-5MD copolymer.

Figure 24. EPR spectrum of PMBA at dose = 0.61 Mrad.

Figure 25. EPR spectrum of P(MMA-MBA) at dose = 0.45 Mrad.

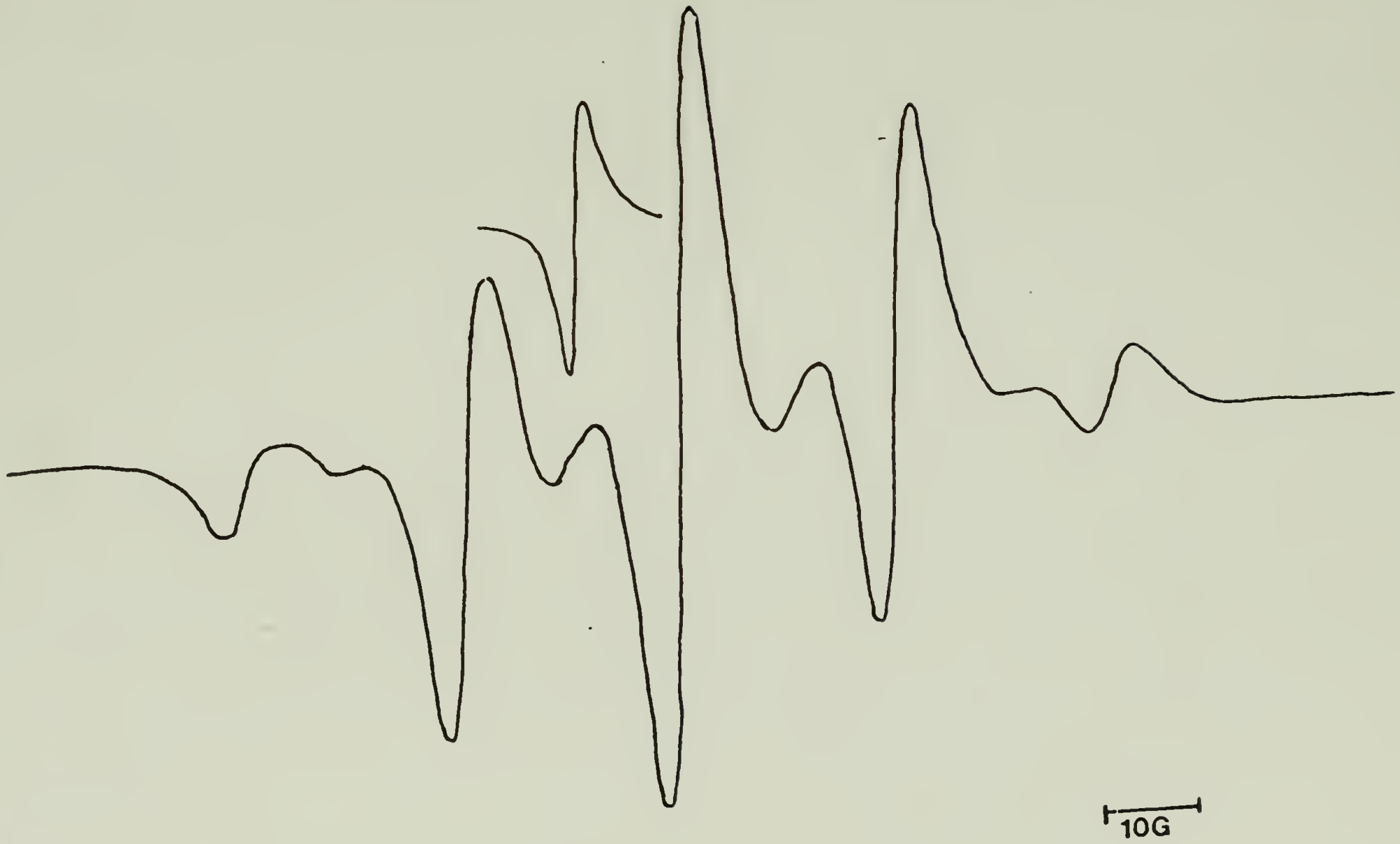

Figure 26. EPR spectrum of P(MMA-DBPMA) at dose = 0.62 Mrad.

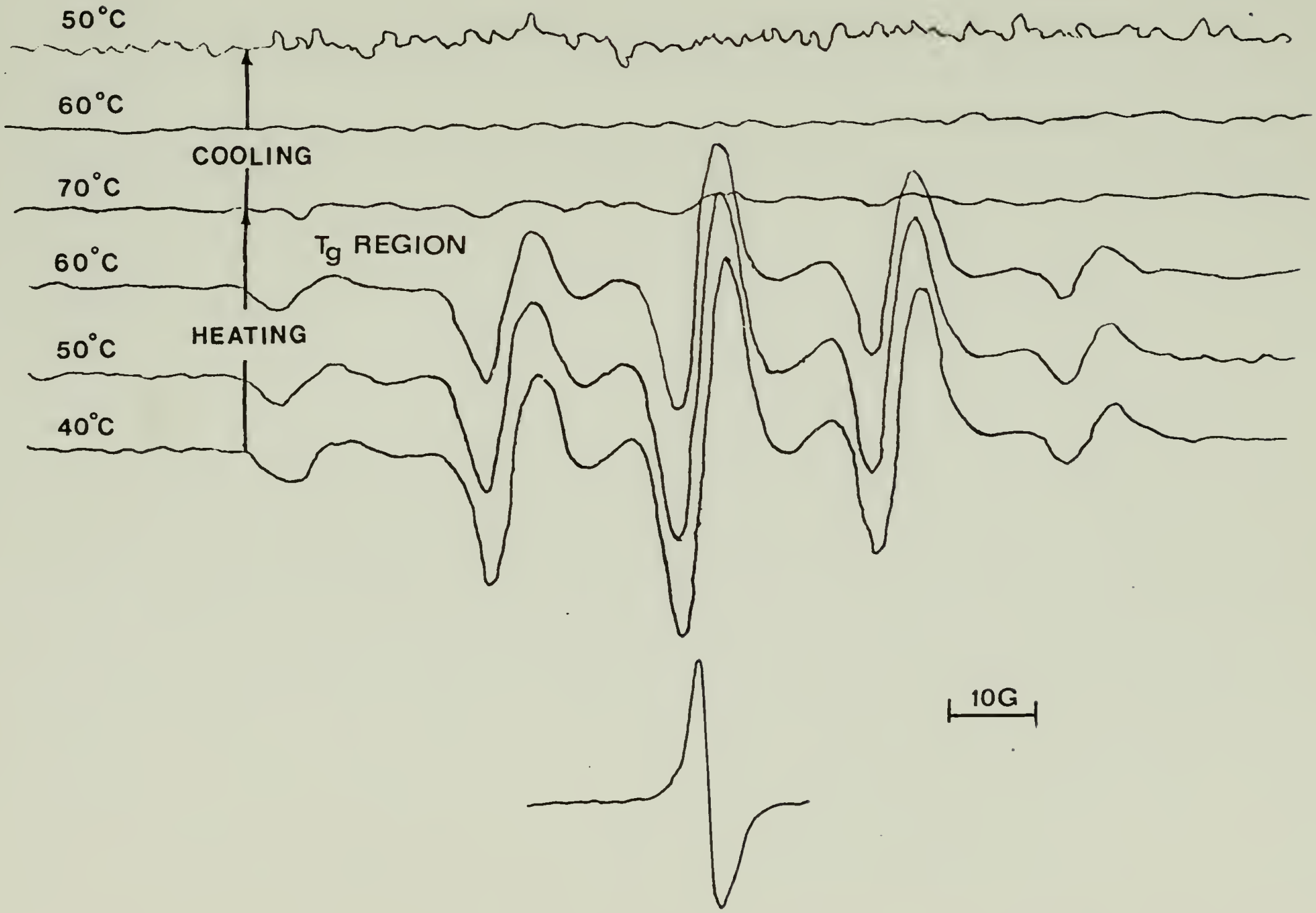

Figure 27. EPR spectra of irradiated P(MMA-DBPMA) as a function of temperature.

EPR spectra of PMBA, P(MMA-MBA), P(MMA-DBPMA) are given in Fig. 24 and 25 and 26. Fig. 27 shows the EPR spectra of P(MMA-DBPMA) as function of temperature. This shows the T_g region.

Discussion of Results

The homopolymers and copolymers containing MBA or DBPMA show marked differences in their thermal and radiative degradations. They will be important for consideration for their potential applications.

In case of the methyl-α-bromoacrylate systems, the thermograms of poly MBA showed that the first stage of pyrolysis caused ca. 56% weight loss. Two mechanisms are possible. The first is the elimination of CH_3Br, to produce monolactone and/or dilactone:

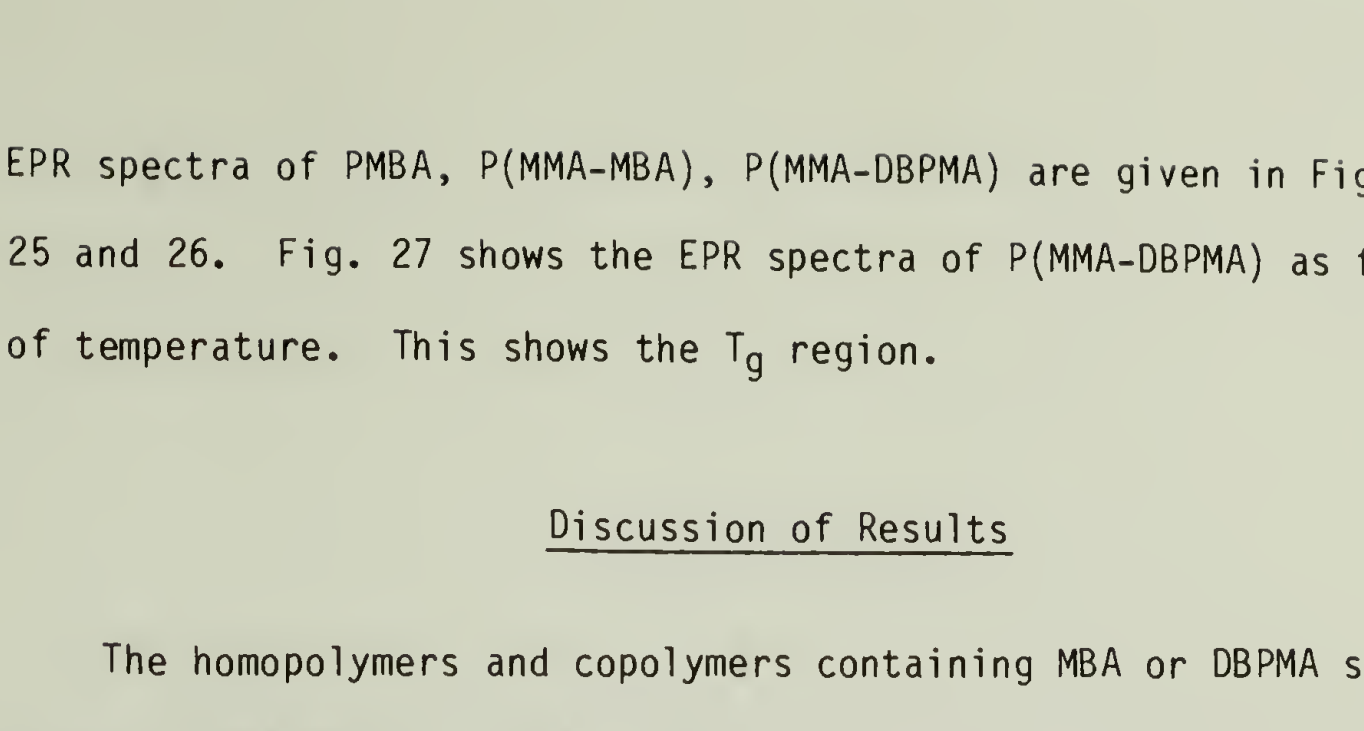

(13)

or HBr elimination:

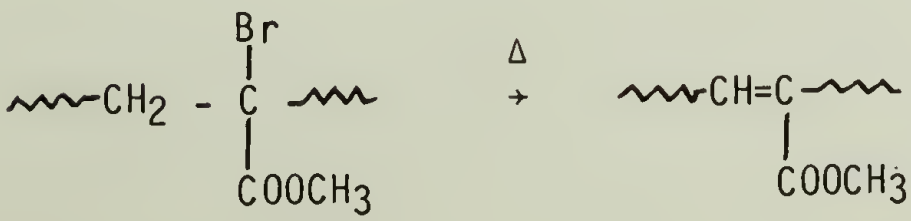

(14)

The observed weight loss for the homopolymer corresponds to an MBA content of 98% according to reaction 13, whereas the MBA content would be about 114% of theoretical if HBr elimination is the dominant mechanism of pyrolysis. This suggests the main low temperature pyrolysis process is the CH_3Br elimination. However, pyrolysis GC-MS needs to be carried out to substantiate the mechanism.

Since PMMA does not have this low temperature pyrolysis process, TGA may be used to determine the MBA contents in poly(MMA-co-MBA). If one assumes %MBA=% wt loss (165/95) for process 13, then the TGA curves in Figure 18 gave the comonomer compositions for MBA in good agreement with those determined by elemental analysis (Table 8).

Radiolysis of homopolymer of MBA results primarily in crosslinking. Therefore, G_s and G_x values cannot be determined by the present methods (Table 10). The G_{rad} value is very high ~7. The process involved is likely to be the severence of the C-Br bond, followed by intermolecular hydrogen abstraction and crosslinking:

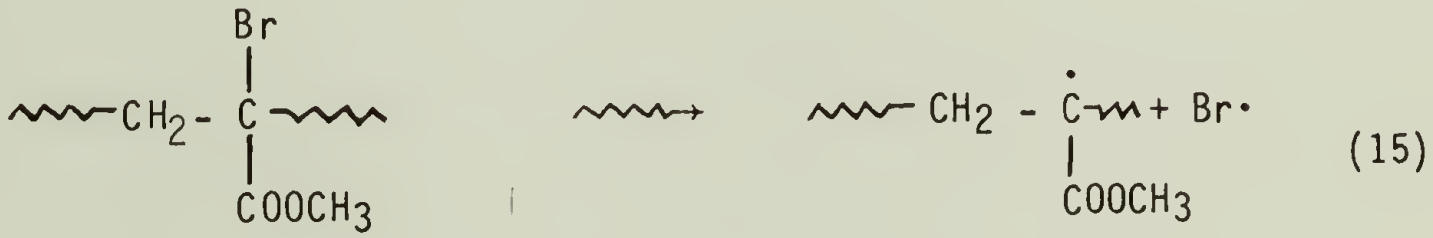

(15)

(I)

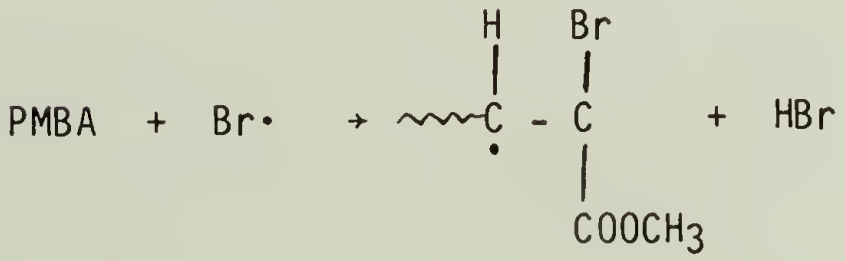

(16)

(II)

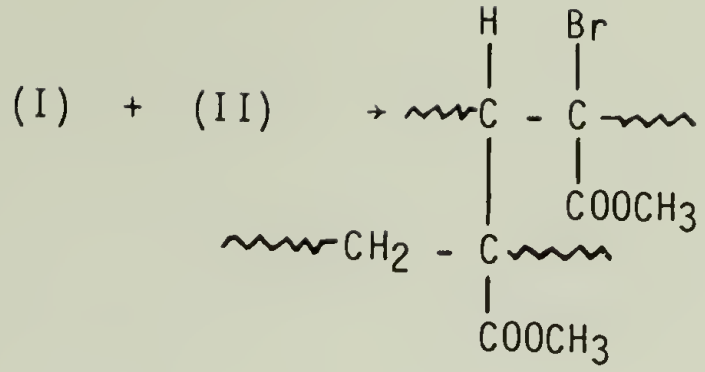

(17)

The primary radical (I) was seen as the five-line EPR species. However, some dissociation of the primary radical also occurs as indicated by the three line EPR spectra of a macroradical (II) resulting from radiolysis.

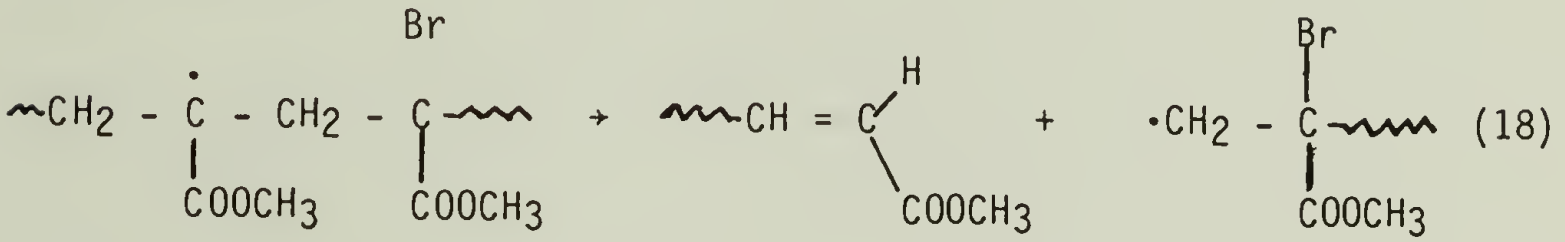

(18)

(III)

As the content of MBA decreases in the copolymer, it is possible to determine scission and crosslinking G values because the former process involving the MMA monomer units dominates the radiolysis leading to predominantly chain scission. Furthermore, G_{rad} also decreases rapidly indicative of the fact that the weak C-Br bonds and the higher atomic number for Br contribute toward higher sensitivity of the MBA monomer units to radiolysis (Table 9). This fact is reflected in G_S values for the copolymer which are always much greater than that for PMMA. Nevertheless, the occurrence of crosslinking renders the copolymers undesirable in positive resist applications.

These EPR results also suggest that it is the MBA diads on the chain in copolymers which give triplets with hyperfine splitting. The electron withdrawing effect and the bulkiness of bromine groups not only makes the quarternary carbon more susceptible to radiolysis, but should also make the resultant $\sim CH_2-\dot{C}(Br)COOCH_3$ radical more susceptible to attack by neighboring groups. The hyperfine splitting patterns of PMBA and P(MMA-MBA) copolymers are consistent with the mechanism described above. Some of the G_{rad} values agree with the G_s values obtained from molecular weight measurements. A final remark about the radiolysis of poly(MMA-Co-MBA) is that the characteristic nine-line spectrum of MMA was never observed even when MBA is present at only 3 mole percent. Therefore, the primary radiolysis process is that of reactions 15 and 18.

The placement of bromine atoms in the pendant groups in DBPMA alters much of the thermal and radiolysis properties described above for MBA where the Br is on the backbone. Though the TGA of the copolymers of MMA and DBPMA also show two distinct stages, the initial one occurs at much higher temperatures than the MBA copolymers (Table 7). The second stage occurs only about 30-40°C higher and the two processes are not very distinct in the copolymers (Figure 19). They are clearly discernible only in the homopolymer of DBPMA. The present interpretation is that at 360°C there is depolymerization of this sterically hindered monomer. At higher temperatures ester decomposition becomes significant. The ester decomposition is

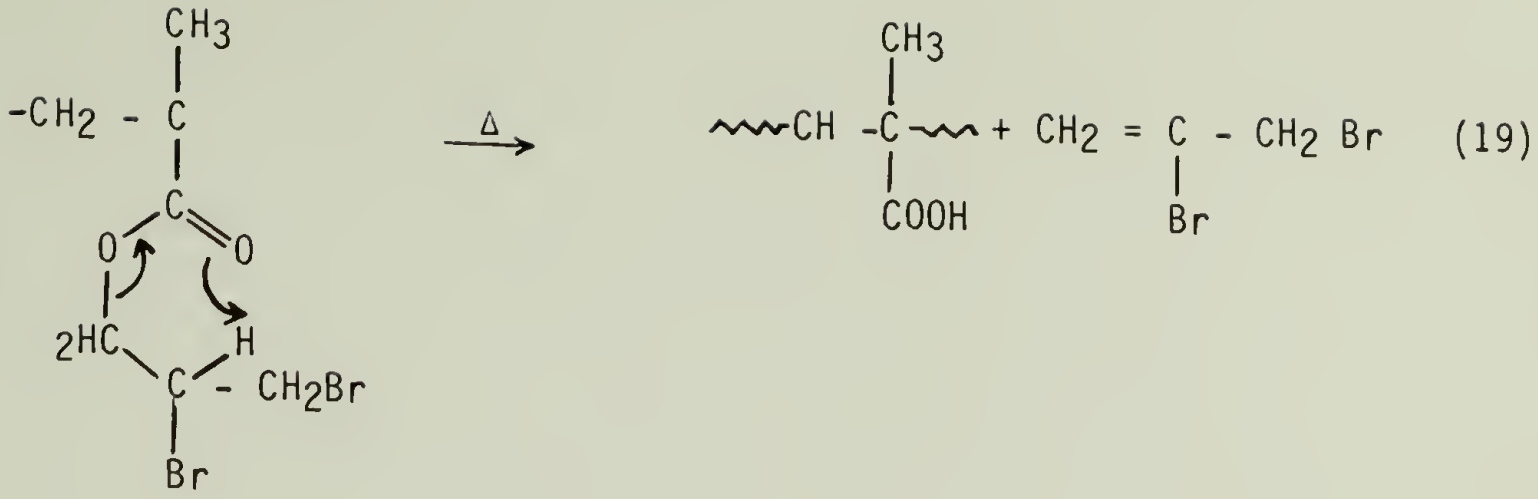

(19)

followed by decarboxylation of the methacrylic acid units.

The surprising observation is that the pyrolysis of poly(MMA-Co-DBPMA) is complete at lower temperatures than poly(MMA-Co-MBA) at low m_2 content. This may be a manifestation of greater steric hinderance in DBPMA. The copolymer degrades more readily with high m_2 contents.

The radiolysis results of poly(MMA-Co-DBPMA) is particularly interesting. First of all, the G_{rad} value at high m_2 is comparable to PMBA in support of the greater susceptibility of the scission of the C-Br bond irrespective of where the Br atom is situated. Secondly, the EPR spectra of irradiated copolymer shows only the characteristic nine-line spectrum of the PMMA units. This is consistent with the expectation that C-Br bond scission here does not lead to the main chain radicals. Finally, crosslinking is the dominant consequence of radiolysis of poly(MMA-Co-DBPMA) for m_2>5 mole fraction.

Consequently, scission of either the β or γ C-Br bond in the pendant group leads largely to abstraction of a proton in the pendant group of another polymer molecule to eliminate HBr and subsequent crosslinking by radical combinations.

In conclusion, the presence of Br atoms either in the backbone or the pendant group enhances the radiolysis sensitivity of the polymer. However, the reactivity of Br atoms toward hydrogen abstraction results in crosslinking reactions thus rendering these materials unsuitable as positive resists. In the case of DBPMA, even the copolymers with low content of DBPMA are difficult to dissolve in any solvent creating problmes in resist applications.

C H A P T E R VII

CHLOROACRYLATES

Results

Homopolymers and copolymers of methyl α chloroacrylate and trichloro ethyl methacrylate with methyl methacrylate were synthesized by procedures outlined in the experimental sections. Compositions were determined by elemental analysis. Reactivity ratios were determined by Fineman-Ross method (28).

TABLE 11

Monomer Reactivity Ratios of MMA-Chloroacrylate Copolymers

System	$r_1 \pm \Delta r_1$	$r_2 \pm \Delta r_2$
MMA-MCA	0.36 ± 0.05	0.26 ± 0.05
MMA-MTC	0.46 ± 0.1	0.13 ± 0.02

Both r_1 and r_2 values for the two systems are less than one indicating the tendency towards alternating polymerization. The preferential addition of MMA over MCA (or TCEMA) monomer to MCA (or TCEMA) radical is attributed to steric factors.

Table 12 lists the copolymers of varying compositions which were used in the evaluation of G values.

TABLE 12

Molecular Weights and Compositions of Chlorine Containing Vinyl Polymers for Degradation Studies

Polymer	m_2-mole %	$\overline{M}_n \times 10^{-5}$	$\overline{M}_w \times 10^{-5}$	$\overline{M}_w/\overline{M}_n$
P(MMA-MCA1)	16	2.814	3.447	1.22
P(MMA-MCA2)	20	2.492	4.024	1.61

P(MMA-MCA3)	42.5	2.110	3.385	1.60
P(MMA-MCA4)	62	1.450	2.490	1.71
P(MMA-MTC1)	9	3.019	4.321	1.43
P(MMA-MTC2)	24	2.192	3.197	1.45
P(MMA-MTC3)	34	1.696	2.634	1.55
P(MMA-MTC4)	38	1.321	2.115	1.60
PTCEMA	100	1.492	2.319	1.55

These polymers were irradiated to different doses and $\overline{M}_n^{-1}$ and $\overline{M}_w^{-1}$ vs. dose plots were constructed to evaluate G_S and G_X values (Fig. 28,29,30,31,32,33,34,35,36). All results are compared to PMMA which gave $G_S = 1.4$ and $G_X = 0$. Table 13 summarizes the G values of the systems studied.

TABLE 13

G_{rad} at 298°K and $G_S - G_X$ Values for γ-Irradiated Chlorine Containing Vinyl Polymer

Polymer	m_2-mole %	G_S-G_X	G_S	G_X	G_{rad}
PMMA	0	1.4	1.4	0	1.42
P(MMA-MCA1)	16	6.46	6.71	0.24	0.98
P(MMA-MCA2)	20	5.37	5.55	0.18	1.56
P(MMA-MCA3)	42.5	4.36	4.82	0.45	3.28
P(MMA-MCA4) (1st 3 pts)	62	1.14	1.14	0	---
PMCA	100	---	---	---	6.07
P(MMA-MTC1)	9	1.42	1.42	0	1.46
P(MMA-MTC2)	24	0.54	0.54	0	1.07
P(MMA-MTC3)	34	1.15	1.15	0	1.0
P(MMA-MTC4)	38	1.23	1.23	0	---
PTCEMA	100	2.07	2.07	0	4.1

Discussion of Results

The data reveals that the P(MMA-MCA) copolymers degrade more efficiently than PMMA reference when γ-irradiated in vacuo. The G values vary with the composition of the comonomer and are not a linear function of the composition.

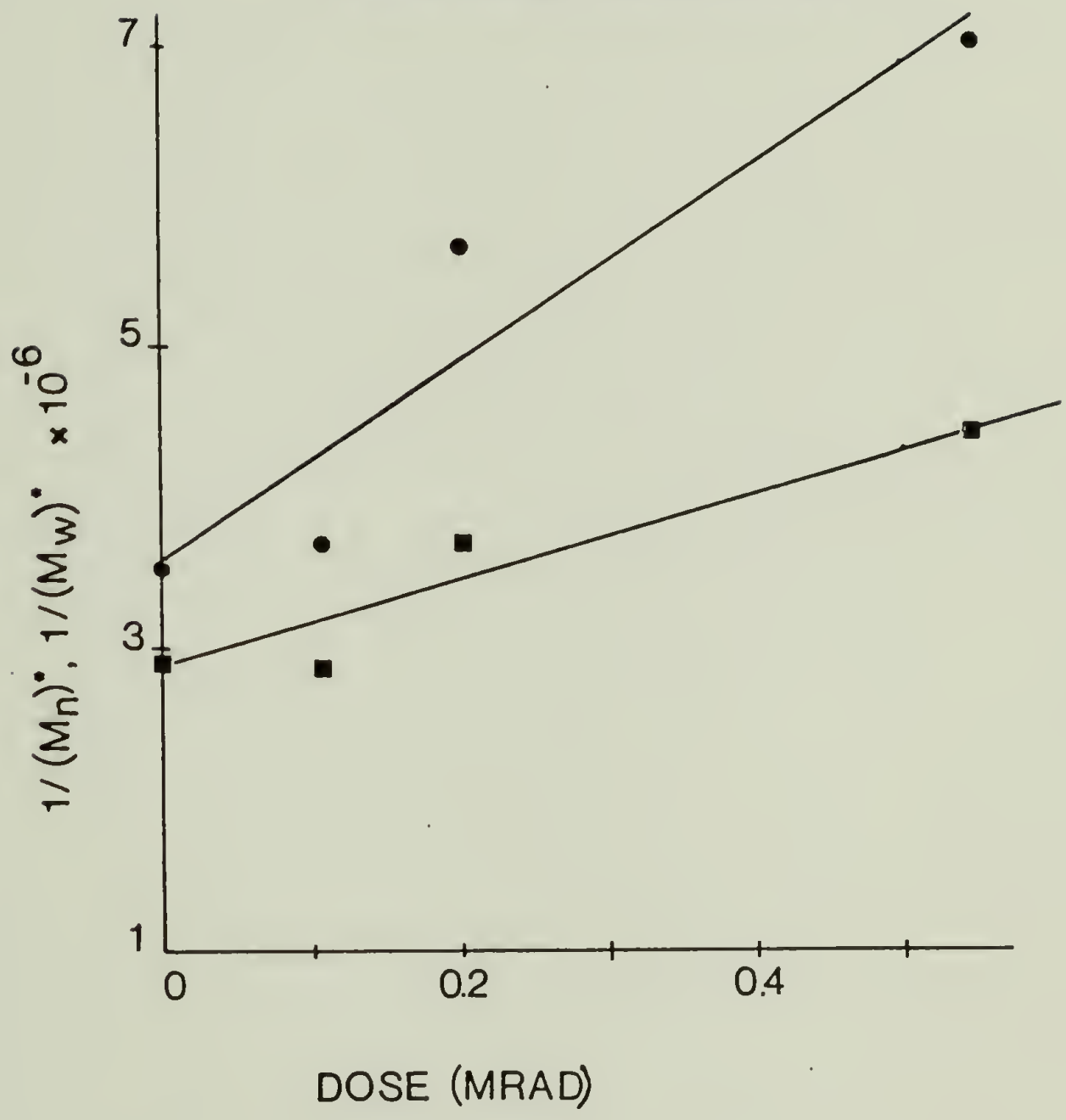

Figure 28. $1/(\bar{M}_n)^*$, $1/(\bar{M}_w)^*$ vs. dose plot for MMA-MCA1 copolymer.

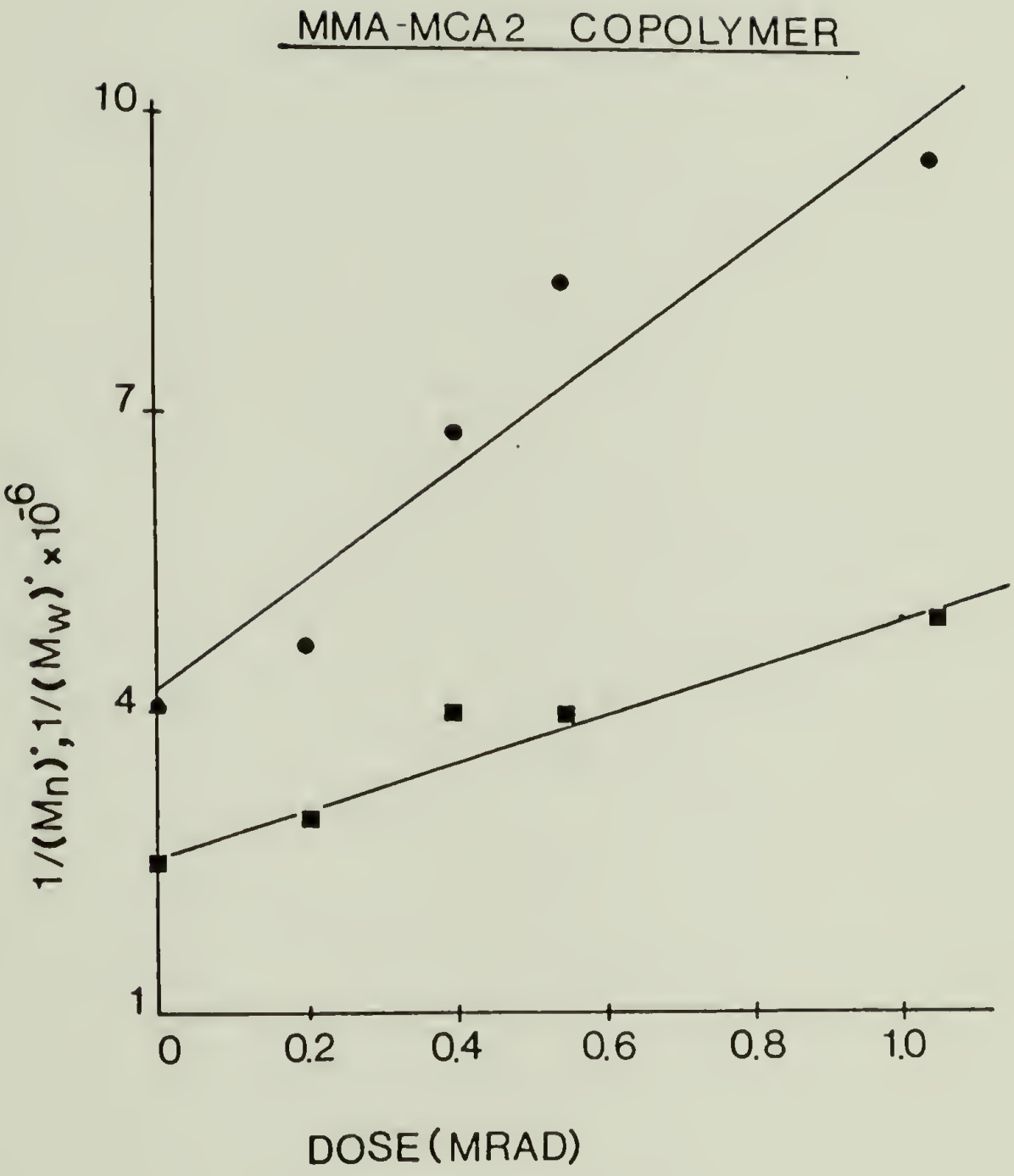

Figure 29. $1/(\bar{M}_n)^*$, $1/(\bar{M}_w)^*$ vs. dose plot for MMA-MCA2 copolymer.

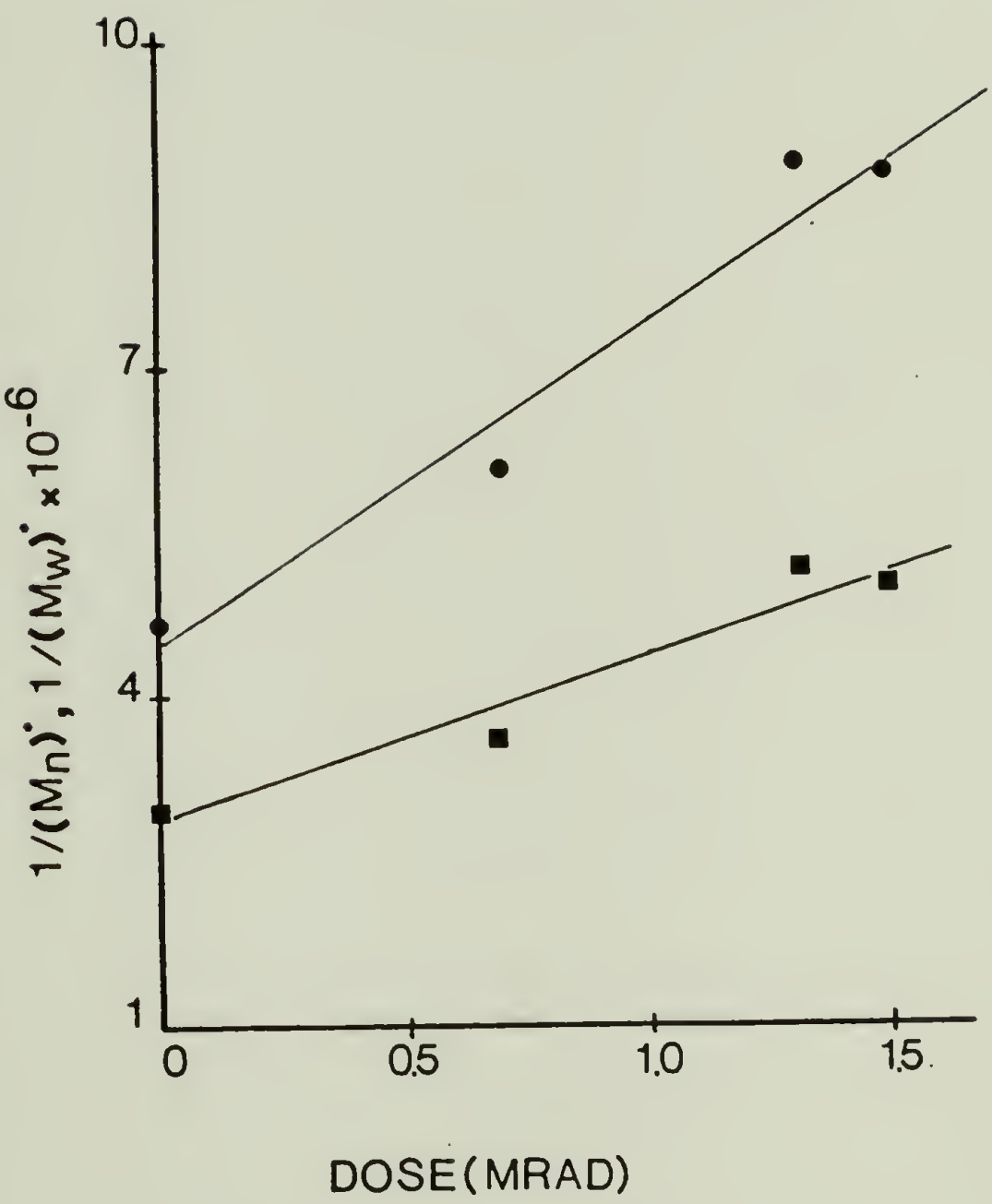

Figure 30. $1/(\bar{M}_n)^*$, $1/(\bar{M}_w)^*$ vs. dose plot for MMA-MCA3 copolymer.

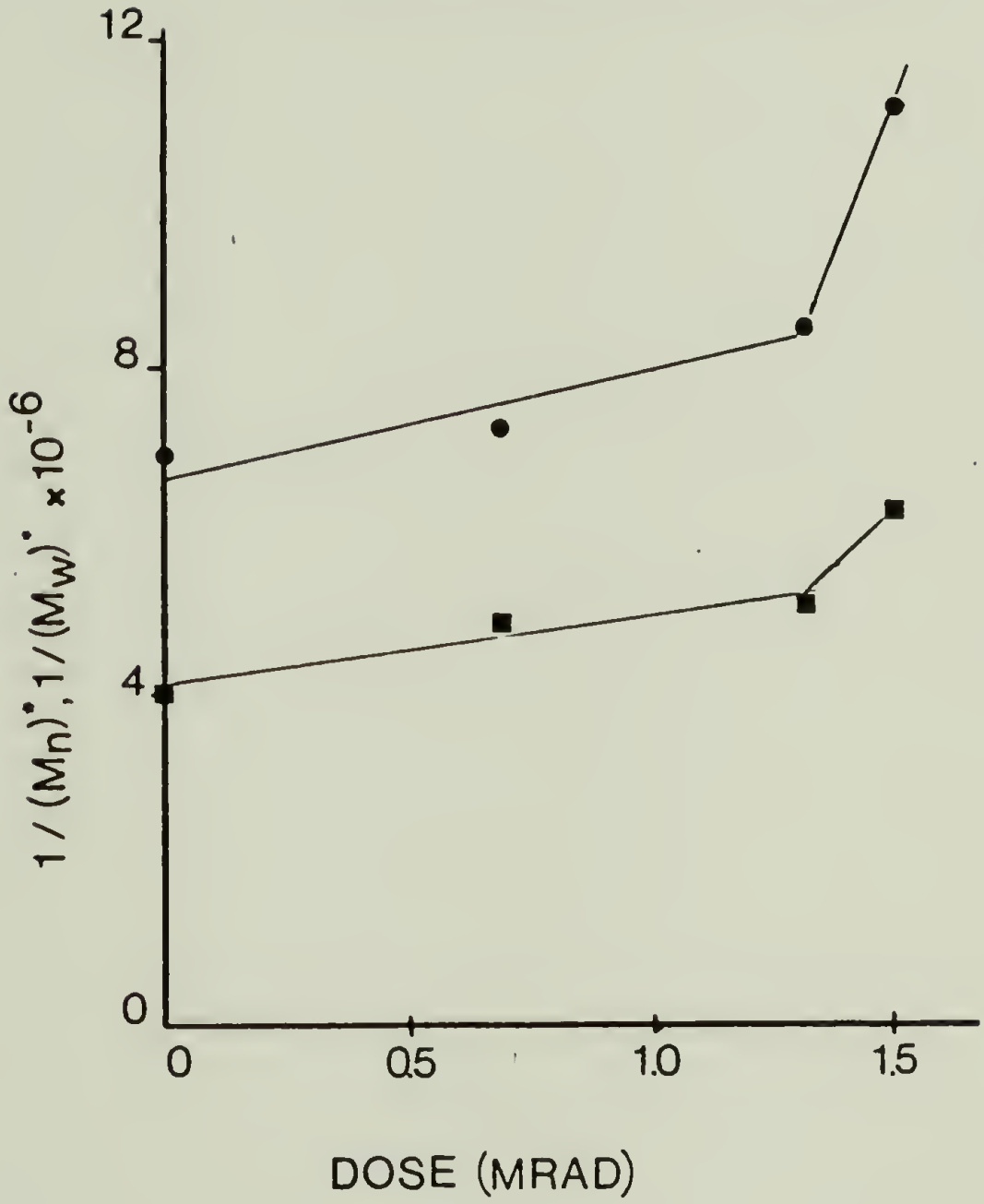

Figure 31. $1/(\bar{M}_n)^*$, $1/(\bar{M}_w)^*$ vs. dose plot for MMA-MCA4 copolymer.

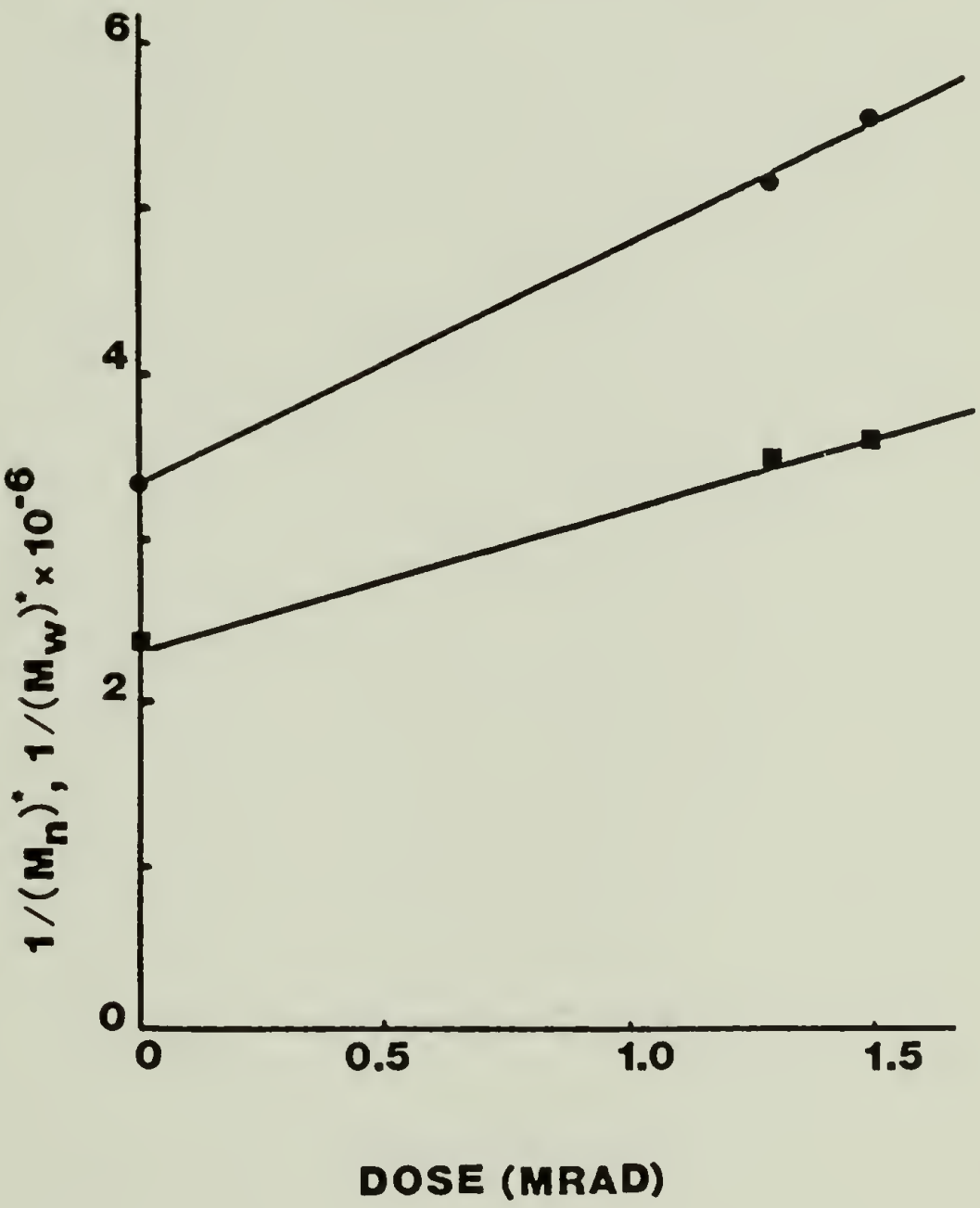

Figure 32. $1/(\bar{M}_n)^*$, $1/(\bar{M}_w)^*$ vs. dose plot for MMA-MTC1 copolymer.

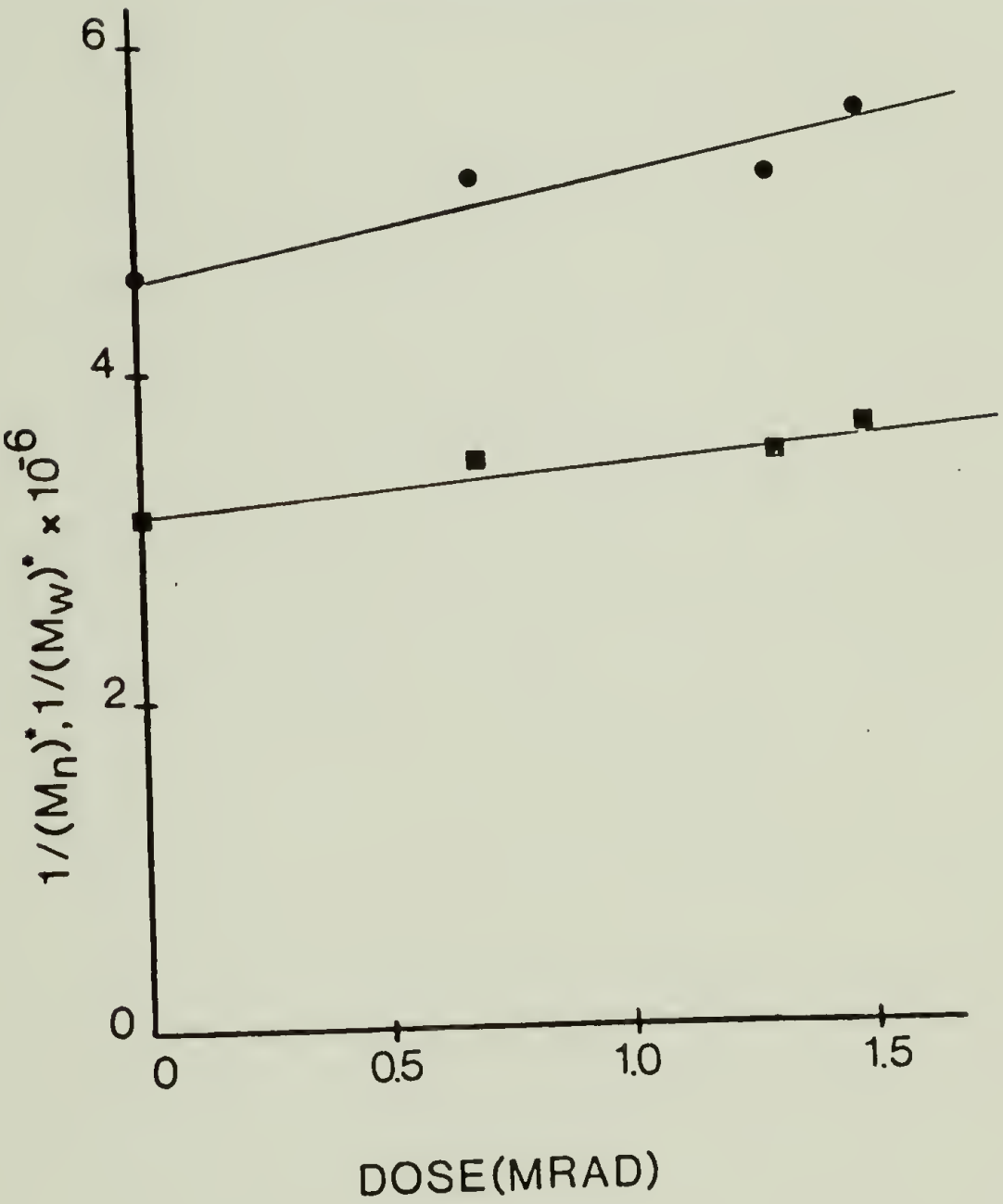

Figure 33. $1/(\overline{M}_n)^*$, $1/(\overline{M}_w)^*$ vs. dose plot for MMA-MTC2 copolymer.

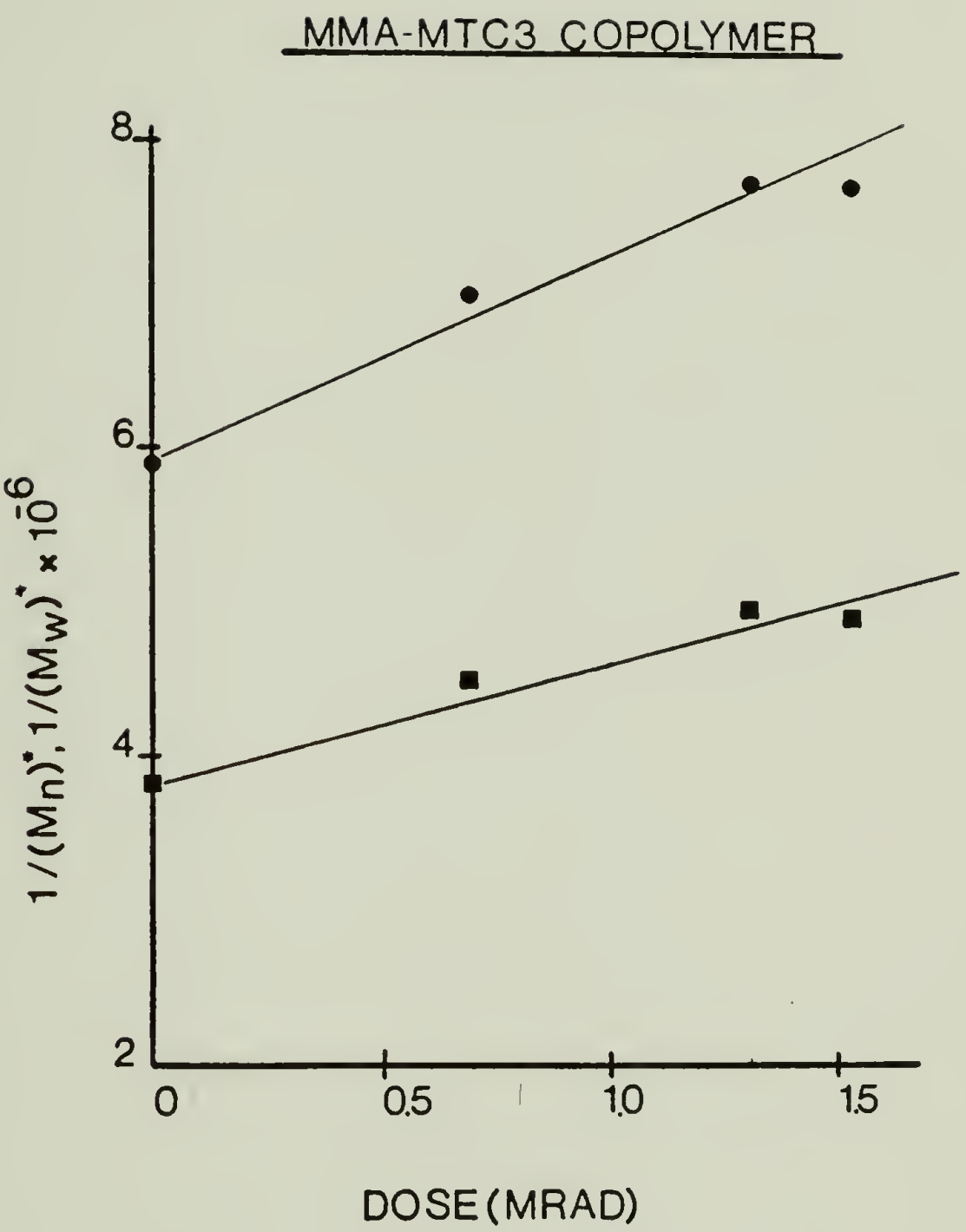

Figure 34. $1/(\bar{M}_n)^*$, $1/(\bar{M}_w)^*$ vs. dose plot for MMA-MTC3 copolymer.

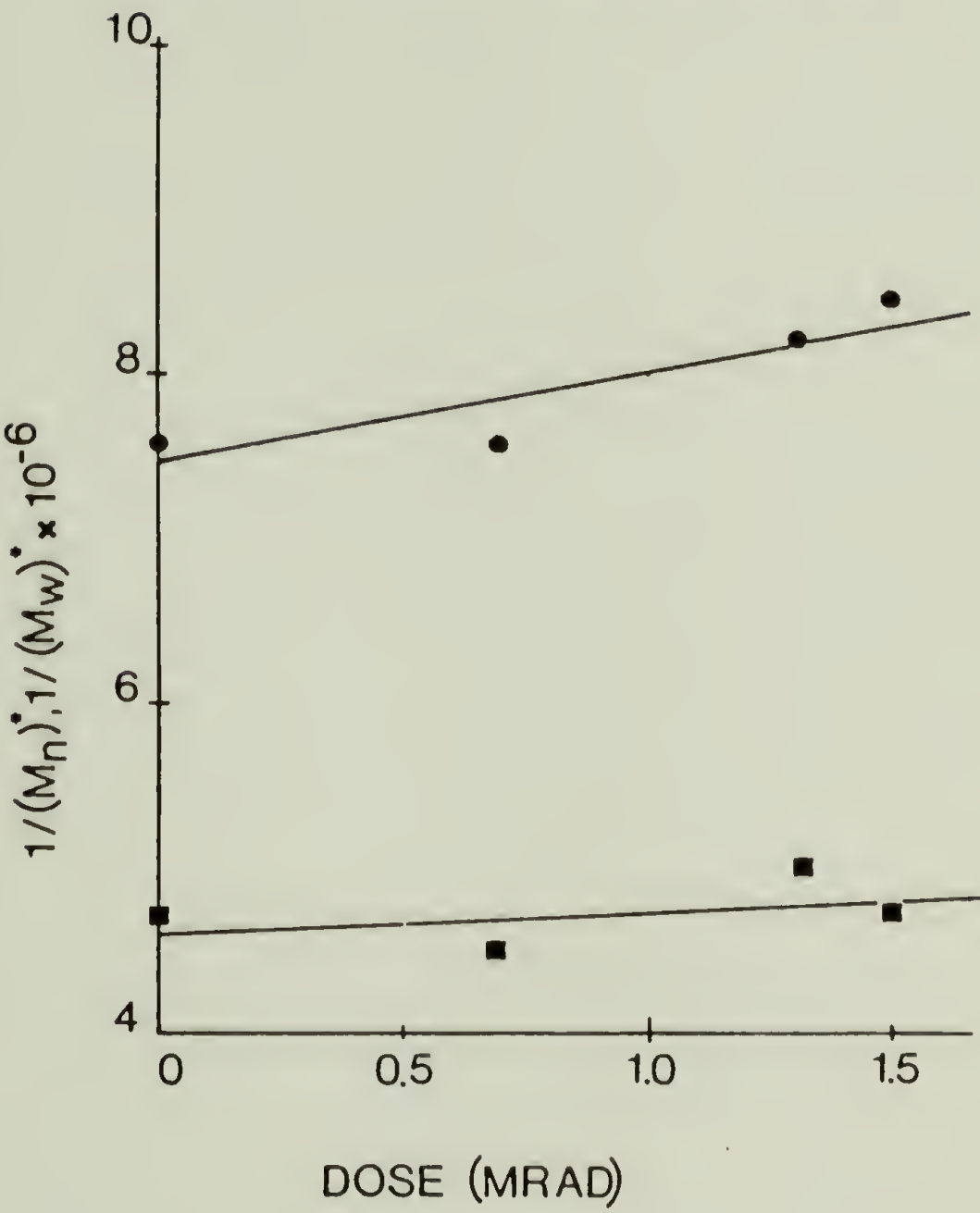

Figure 35. $1/(\bar{M}_n)^*$, $1/(\bar{M}_w)^*$ vs. dose plot for MMA-MTC4 copolymer.

PTCEMA

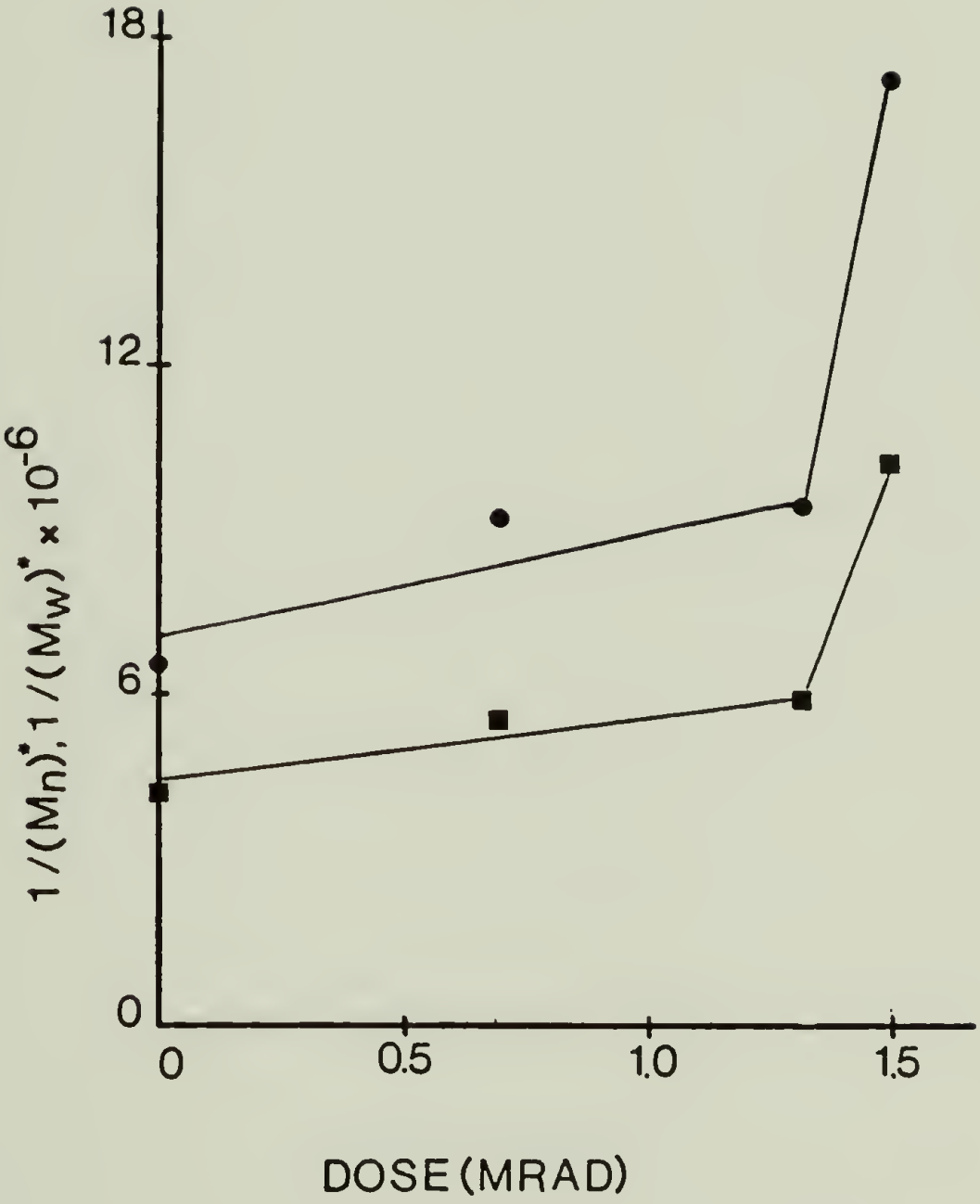

Figure 36. $1/(\bar{M}_n)^*$, $1/(\bar{M}_w)^*$ vs. dose plot for PTCEMA.

The high G_S values may be attributed to the dissociative electron capture which is favorable for chlorine (20). The MTC copolymers show a variation in the G value with the composition change also. There is a change in slope in the $1/\overline{M}_n$ and $1/\overline{M}_w$ vs. dose plots for the homopolymer. This is not seen in case of the copolymers.

The EPR spectrum of γ-irradiated poly(methyl α chloroacrylate) and its copolymers with MMA at 298°K are shown in Fig. 37,38,39. The separation between the two extreme shoulders in PMCA as indicated by arrows is about ~80 G. The two outermost lines are not symmetric indicating anisotropy.

Microwave power saturation measurements (Fig. 40) suggest the presence of more than one type of radical. The position, not relative intensities, of the central five line spectrum with a line width of 11 G suggests interaction with four equivalent protons. This is probably due to the radical shown below:

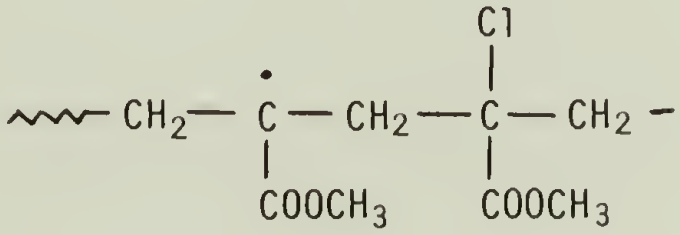

This undergoes subsequent cleavage to give a three line spectrum with a line width of 11G. The following mechanism appears to be the most feasible:

Figure 37. EPR spectrum of PMCA at dose = 0.22 Mrad.

Figure 38. EPR spectrum of P(MMA-MCA) (80.20) at dose = 1.49 Mrad.

Figure 39. EPR spectrum of irradiated P(MMA-MCA) (67.5:42.5).

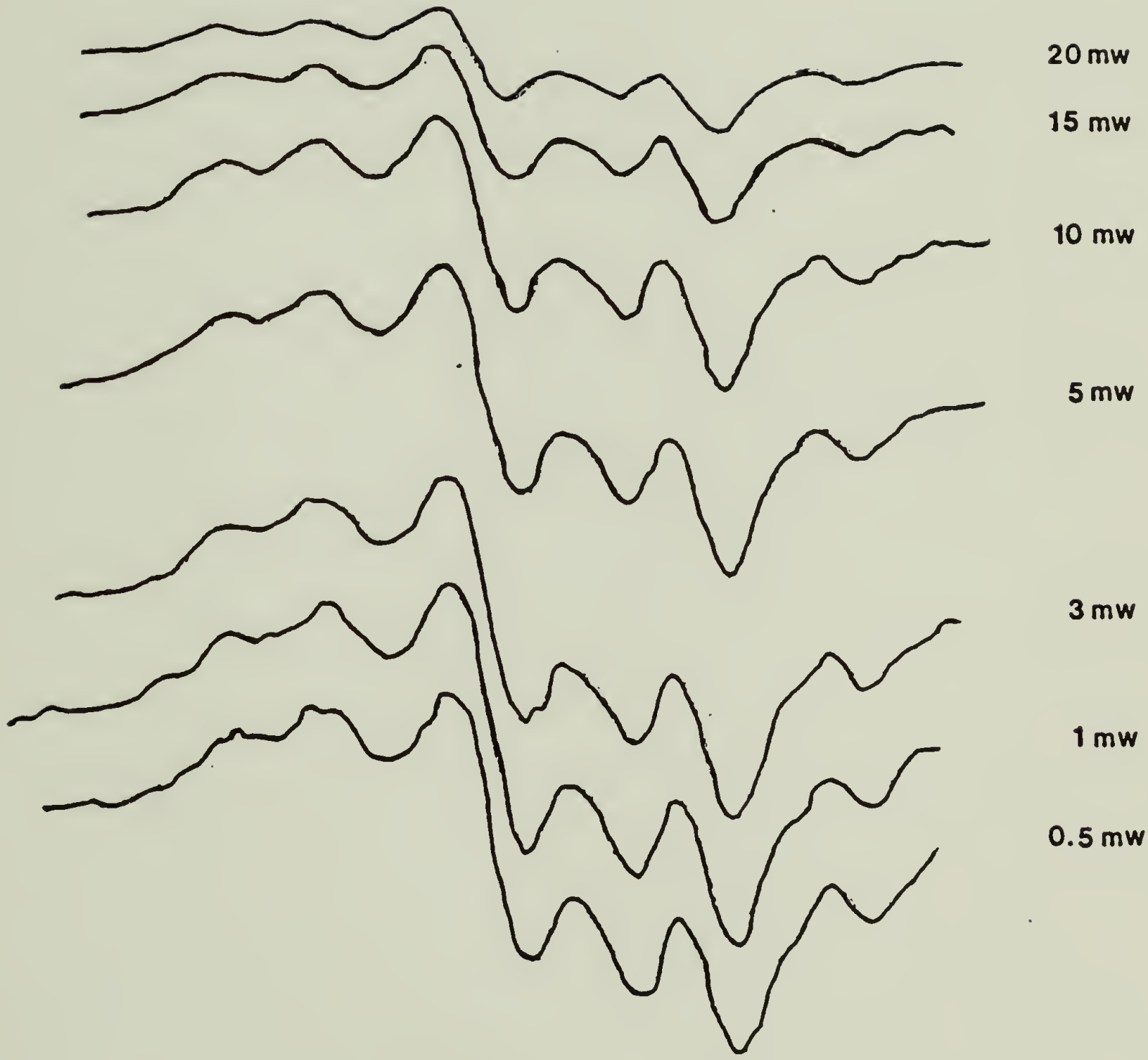

Figure 40. Microwave saturation measurements for PMCA at dose = 0.22 Mrad.

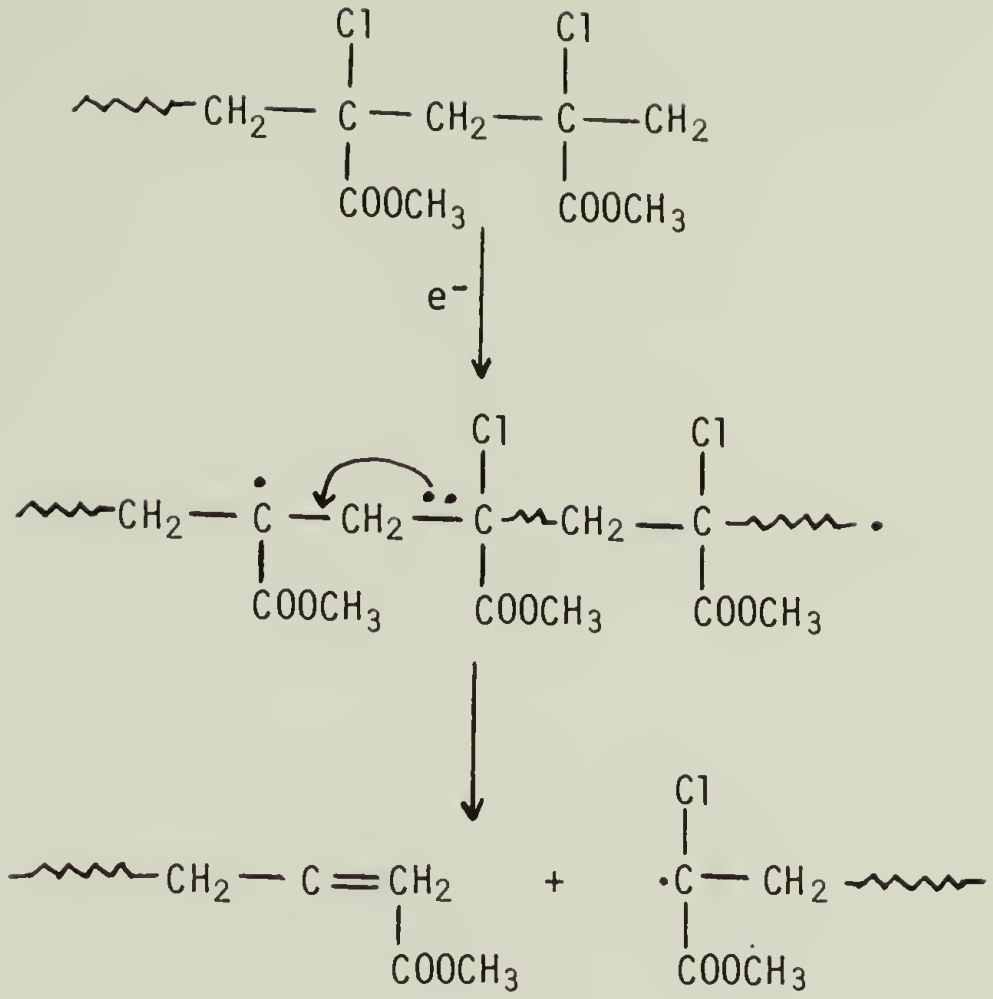

The formation of three line spectrum may also be explained by the following mechanism:

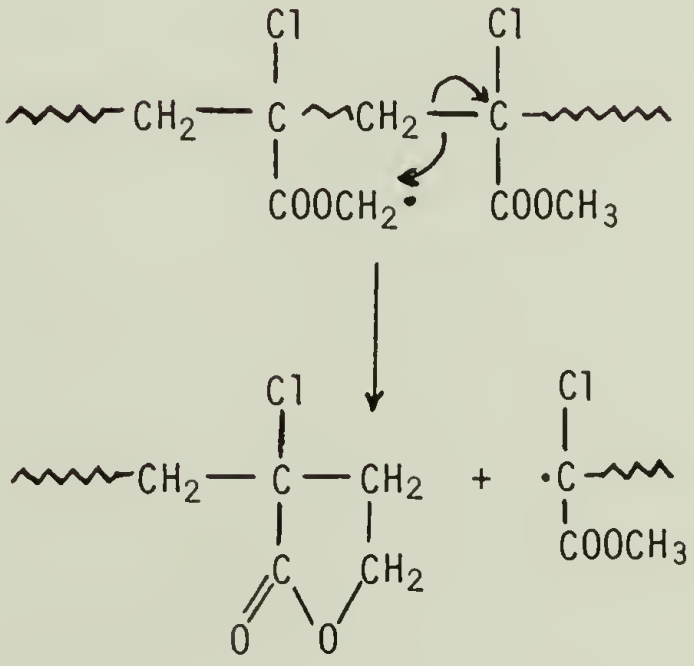

These mechanisms suggest that the cleavage on exposure to γ-radiation occurs in concurrent ways. Product analysis may yield a more accep-

Copolymers of MMA-MCA having 20 mole % of MCA showed a nine line spectrum (Fig. 38) similar to PMMA. However 42.5 mole % of MCA copolymer behaved similar to PMCA (Fig. 39).

This indicates that the probability of diad and triads of PMCA is likely at higher concentrations of MCA in copolymer. This also suggests that diad and triad formations of MCA are necessary for predominant cleavage of the C-Cl bond.

We can summarize the radiation degradation of PMCA and copolymers as follows. Two types of radicals are formed: chain scission radicals in which the main carbon chain backbone is broken and chain radicals in which a side group is lost.

EPR spectra of γ-irradiated P(MMA-MTC) copolymers at 298°K gave a nine line spectrum similar to that of PMMA propagating radical, Fig. 41).

Since this spectrum is obtained from the propagating radical:

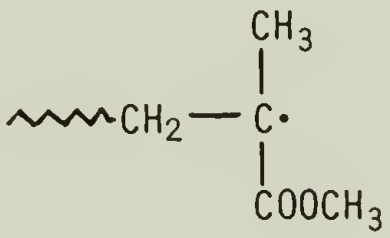

the rupture probably occurs at the MTC comonomer.

Figure 41. EPR spectrum of P(MMA-MTC) at dose - 0.26 Mrad.

C H A P T E R VIII

CONCLUSIONS AND SUGGESTIONS FOR FUTURE WORK

We studied the effects of substrate and irradiation temperature on the G_S value of PMMA. The substrates used were silicon, silicon with a 5000 Å SiO_2 covering layer and boron doped silicon. No significant difference in the G_S values was found for the three cases.

The G_S value of PMMA increased substantially with an increase in the irradiation temperature. Activation energy for the scission process was calculated to be 2.78 kcal/mole as compared to values of 1.0 kcal/mole reported by Charlesby and Moore and 1.58 kcal/mole reported by Wundrich. The increase in G_S at higher temperatures is probably due to the "cage effect". Reactive intermediates, formed during irradiation, are held together closely in the solid and may recombine. At higher temperatures, the possibility of recombination is much lower due to diffusion. Therefore, the probability of scission becoming permanent increases at higher temperatures.

The G_S and G_X values were evaluated for the homopolymers and copolymers of methyl α bromoacrylate and 2,3-dibromo propyl methacrylate with MMA. The homopolymers crosslinked on γ ray irradiation. P(MMA-MBA) and P(MMA-DBPMA) degraded more efficiently than PMMA when γ irradiated in vacuo. This implies that the presence of Br atoms either on the backbone or the pendant group increases the radiation sensitivity of the polymer. This effect is more pronounced with the increasing content of the bromoacrylate comonomer. A significant amount of crosslinking (with G_X in the range of 0.21 - 0.65) takes

place in these copolymers because of the tendency of the Br atom to abstract hydrogen. Therefore these copolymers are unsuitable as positive resists.

G_S and G_X values were evaluated for the homopolymers and copolymers of methyl α chloroacrylate (MCA) and trichloro ethyl methacrylate (TCEMA) with MMA. On irradiation, the MMA-MCA copolymers degrade mainly by chain scission, although the G_X values are also significant. At low levels of irradiation, the MMA-MCA copolymer with 16 mole % MCA has the highest G_S value ~ 6.7. The G_S value decreases with a further increase in the MCA content. The rate of crosslinking associated with the comonomer is lower for the copolymer when compared to the homopolymer because of the random distribution of the MCA units along the chain. This reduces the probability of reaction of two MCA radicals to form a crosslink. For both the homopolymer of TCEMA and it's copolymers with MMA, the G_X values are zero. The G_S values do not vary linearly with the composition.

EPR data were used to propose mechanisms for the scission and crosslinking processes taking place in these systems. They need to be substantiated with product analysis from gas chromatography and mass spectrometry.

There needs to be a further systematic investigation of structurally related polymers in order to establish the relationship between G_S and G_X values and the copolymer composition. G_S and G_X values of those copolymers should be evaluated as a function of irradiation temperature particularly at or above the ceiling temperature.

Finally, it is important to evaluate the G_S and G_X values of these copolymers using an electrom bean to evaluate their utility as electron beam resists.

REFERENCES

1. D.W. Hess, Chem. Tech., 423, July (1979).
2. George Brewer, "Electron Beam Technology in Microelectronic Fabrication", Ed., George Brewer, Academic Press, Chapter 1.
3. M. Hatzakis, Polymer Eng. and Science, 14, 516 (1974).
4. M. Hatzakis, C. Ting and N.S. Vishvanathan, Proc. 6th International Conference on Electron and Ion Beam Technology, R. Bakish, Ed., Electrochemical Society, Princeton, N.J., 1975, p. 542.
5. L.F. Thompson and R.E. Kerwin, Annu. Rev. Mater. Sci., 6, 267, (1976).
6. M. Hatzakis, J. Vac. Sci. Technol., 12, 1276 (1975).
7. R.A. Harris, J. Electrochemical Soc. Solid State Science and Technol., 270 (1973).
8. A. Charlesby and N. Moore, Int. J. Appl. Rad. Isotopes, 15, 703 (1964).
9. F.R. Boyer and R.S. Spencer, Adv. Coll. Sci., 2, 1 (1946).
10. L.A. Wall and D.W. Brown, J. Phys. Chem., 61, 129 (1957).
11. K. Wundrich, J. Polym. Sci. (Polymer Physics), 12, 201 (1974).
12. J. Kroh and A. Polowinska, Bullt. Polo. Sciences, Vol. XVI, No. 8, 425 (1968).
13. L.F. Thompson, Solid State Technol., 17, 44 (August, 1974).
14. I. Haller, M. Hatzakis and R. Srinivasan, IBM J., 12, 251 (1968).
15. T. Kitahohji, Y. Yoneda et al., Electrochemical Society Meeting, Pittsburgh, Extended Abstracts, Vol. 78(2), 472 (1978).

16. C.U. Pittman, Jr., Chi-Yu Chen, Mitsuru Ueda et al., J. Polym. Sci., Polymer Chem. Ed., 18, 3413 (1980).

17. J.N. Helbert, Chi-Yu Chen, C.U. Pittman, et al., Macromolecules, 6, 1104 (1978).

18. J.N. Helbert, B.E. Wagner, P.J. Caplan and E.H. Poindexter, J. Appl. Polym. Sci., 19, 1201 (1975).

19. J.H. Lai, L.T. Shepherd, R. Ulmer and C. Griep, Polymer Eng. and Sci., 17, 402 (1977).

20. J.H. Lai and S. Shrawagi, J. Appl. Poly. Sci., 22, 53 (1978).

21. J.N. Helbert, G.J. Iafrate, C.U. Pittman, Jr., and J.H. Lai, Polymer Eng. and Sci., 20, 1077 (1980).

22. W.H. Hamill in "Radical Ions", E.T. Kaiser and L. Kevan, Ed., Interscience, N.Y. (1967) Chapter 9.

23. J.H. Lai, L.T. Shepherd, R. Ulmer and C. Griep, Proceedings of 4th Photopolymer Conf. Soc. Plast. Eng., Ellenville, N.Y., October (1976).

24. C.Y. Chen, C.U. Pittman, Jr., and J.N. Helbert, J. Polym. Sci. Polymer Chem. Ed., 18 169 (1980).

25. C.U. Pittman, Jr., Easley Wallace, Jr., et al., Proceedings of the IUPAC 28th Macromolecular Symposium, Amherst, July (1982).

26. T. Tada, J. Electrochem. Soc., 134, 1635 (1979).

27. J.H. Lai, J.H. Kwiatkowski and C.F. Cook, Jr., Proceedings of the IUPAC 28th Macromolecular Symposium, Amherst, July (1982).

28. M. Fineman and S.D. Ross, J. Polym. Sci., 5, 259 (1950).

29. N. Grassie, "Chemistry of High Polymer Degradation Processes", Butterworths, London (1956).

30. ASTM D 1671-72.

31. ASTM D 2568.

32. R.D. Heidenreich, L.F. Thompson, E.D. Feit and C.M. Melliar Smith, J. Appl. Phys., 44, 4039 (1973).

33. J.S. Greeniech, "Electron Beam Technology in Microelectronic Fabrication", G.L. Brewer, Ed., Academic Press, Chapter 2.

34. W. Ehrenberg and D.E.N. King, Proc. Roy. Soc., 81, 751 (1963).

35. V.E. Cosslett and R.N. Thomas, Brit. J. Appl. Phys., 16, 779 (1965).

36. L.V. Spencer, "Energy Dissipation by Fast Electrons", Nat. Bur. Stds. (U.S.) Monograph, No. 1, (U.S. G.P.O., Washington, D.C., 1959).

37. R.J. Hawryluk, A.M. Hawryluk and H.I. Smith, J. Appl. Phys., 45, 2551 (1974).

38. A. Cole, Rad. Res., 38, 7 (1969).

39. R.D. Heidereich, J. Appl. Phys., 48, 1418 (1977).

40. H.Y. Ku and L.C. Scala, J. Electrochem. Soc., Solid State Sci. and Technol., 116, 980 (1969).

41. R.W. Kilb, J. Phys. Chem., 63, 1838 (1959).

42. M. Dole, "The Radiation Chemistry of Macromolecules, Vol. II, Academic Press, Chapter 6.

43. R. Lenk, Czech. J. Phys., B12, 876 (1961).

44. J. Kircher, F.A. Slimers, R.A. Markle et al., J. Phys. Chem., 69, 189 (1965).

45. R. Kourim and K. Vacek, Trans. Faraday Soc., 61, 415 (1964).

46. M.C.R. Symons, J. Chem. Soc., 277 (1959).

47. M.C.R. Symons, J. Chem. Soc., 1186 (1963).

48. J. Sohma, T. Komatsu et al., J. Polym. Sci. Part B, 3, 287 (1965).

49. A.A. Miller, E.J. Lawton and J.S. Balwit, J. Polym. Sci., 14, 503 (1954).

50. L.E. Nielsen, "Mechanical Properties of Polymers", Reinhold (1962).

51. L.A. Wall, J. Polym. Sci., 17, 141 (1955).